

A MICROMECHANICS METHOD TO PREDICT
THE FRACTURE TOUGHNESS OF CELLULAR MATERIALS

By

SUKJOO CHOI

A THESIS PRESENTED TO THE GRADUATE SCHOOL
OF THE UNIVERSITY OF FLORIDA IN PARTIAL FULFILLMENT
OF THE REQUIREMENTS FOR THE DEGREE OF
MASTER OF SCIENCE

UNIVERSITY OF FLORIDA

2002

Copyright 2002

by

Sukjoo Choi

This dissertation is dedicated to my parents, Sunggu Choi and Jinsil Yang

ACKNOWLEDGEMENTS

I am very grateful to Dr. Bhavani V. Sankar for providing me the opportunity to complete my M.S. studies under his exceptional guidance and financial support. He is not only my academic advisor but also a great influence in my life. Throughout this research, I have greatly appreciated his consistent encouragement, patience and positive attitude. Also, I would like to thank to Dr. Chen-Chi Hsu, graduate coordinator, for his advice. Because of great help and advice, studying here was a delightful experience.

Many thanks should go to my colleagues, Donald Myers, Nicoleta Apetre and Huadong Zhu. Moreover, I would like to thank my school seniors, Jongyoon Ok, Chungsoo Ha and Kilsoo Mok, who provided me invaluable academic feedback, encouragement and companionship. I would like to thank my girlfriend, Sungshin Kang, who allowed me to devote myself to studying. I would like to express my deepest appreciation to my parents for continuous support and love. I am also thankful to God for giving me the opportunity to extend my education at the University of Florida.

TABLE OF CONTENTS

	<u>page</u>
ACKNOWLEDGEMENTS.....	iv
LIST OF TABLES.....	vii
LIST OF FIGURES	viii
ABSTRACT.....	xi
 CHAPTER	
1 INTRODUCTION	1
2 ELASTIC CONSTANTS OF THE FOAM	4
Formulation of Micro-Mechanics Properties.....	4
Finite Element Verification of Analytical Models.....	7
3 FINITE ELEMENT METHODS OF FRACTURE TOUGHNESS	11
Boundary Displacement at a Crack Tip	11
Model Setup	12
Convergence Analysis for Mode I	13
Mode I Fracture Toughness of Open Cell Foam	17
Mode II Fracture Toughness of Open Cell Foam	19
Fracture Toughness of Mixed Mode on Open Cell Foam	20
Formulation of Fracture Toughness for Mode I and Mode II.....	22
Analytical Model for Mode I Fracture Toughness	22
Analytical Model for Mode II Fracture Toughness	25
Mode I and Mode II Fracture Toughness with Angled Crack	26
Prediction of the Maximum Strength under Tensile Loading	27
Prediction of the Maximum Strength under Shear Loading	29
Mode I Fracture Toughness of Inclined Cracks.....	31
4 FRACTURE TOUGHNESS OF CARBON FOAM.....	34
Material Properties of Carbon Foam.....	34
Mode I Fracture Toughness Test (4-Pt. Bending Tests).....	34
Finite Element Analysis of Fracture Toughness	38

Unit Cell of Carbon Foam – Solid Model.....	38
Micromechanics Analysis for Young’s Modulus and Shear Modulus	39
Unit Cell of Carbon Foam – Beam Model.....	43
Fracture Toughness Estimation of the Solid Model	44
Fracture Toughness of the Beam Model.....	45
5 RESULTS AND DISCUSSION	47
Elastic Constants of Open-cell Foam.....	47
Numerical Analysis of Fracture Toughness.....	47
Fracture Toughness with an Angle Crack.....	48
Fracture Toughness of Carbon Foam.....	48
APPENDIX	
A ANALYTICAL METHOD TO ESTIMATE THE SOLIDITY OF SOLID MODEL ..	50
B CRACK TIP DISPLACEMENT FIELDS FOR ORTHOTROPIC MATERIAL.....	52
REFERENCES	55
BIOGRAPHICAL SKETCH	56

LIST OF TABLES

<u>Table</u>	<u>page</u>
1.1 Material properties of the Zoltex carbon fiber.....	3
3.1 Foam model properties for convergence analysis.....	13
4.1 Mechanical properties of carbon foam	34
4.2 Densities of various forms of carbon	34
4.3 Fracture toughness with specimen properties of carbon foam.....	36
5.1 Constants of fracture toughness curves.....	48
5.2 Results of fracture toughness	49

LIST OF FIGURES

<u>Figure</u>	<u>page</u>
1.1 SEM images of low (left) and high (right) density carbon foam	2
1.2 The packing of polyhedra to fill space: tetrakaidecahedra	2
1.3 Open rectangular cell model	3
2.1 Applied stress for a open-cell foam	4
2.2 Deformed shape of struts on open-cell foam	5
2.3 Stress distribution of tensile loading on open-cell foam.....	8
2.4 Shear applied on open-cell foam.....	9
2.5 Stress distribution of shear loading on open-cell foam.....	9
3.1 Open-cell foam model with a crack	12
3.2 Variation of fracture toughness with various model sizes	14
3.3 Axial stress variation from a crack tip for various model sizes	15
3.4 Log-log plot of axial stress along a crack tip for various model sizes.....	16
3.5 Fracture toughness in various crack lengths	17
3.6 Stress distribution of Mode I fracture ($c=200 \mu\text{m}$, $h=20 \mu\text{m}$)	18
3.8 Stress distribution of Mode II fracture ($c=200\mu\text{m}, h=20\mu\text{m}$)	19
3.9 Numerical result of fracture toughness for Mode II	20
3.10 Stress distribution on the mixed mode fracture ($c=200\mu\text{m}$, $h=20\mu\text{m}$).	21
3.11 Mixed mode fracture toughness of constant length of cell edges	21
3.12 Mixed mode fracture toughness of constant cell wall thickness.....	22

3.13 Crack tip forces and moments in the actual foam and corresponding crack tip stresses in the idealized homogeneous continuum	22
3.14 Variation of α (l/c) with relative density for Mode I.....	25
3.15 Variation of α (l/c) with relative density for Mode II.....	26
3.16 Forces in a ligament under combined loading	27
3.17 Variation of maximum tensile stress σ_y as a function of angle between the xy coordinate system and the principal material directions.....	29
3.18 Variation of maximum shear stress (shear strength) as a function of angle between the xy coordinate system and the principal material directions	31
3.19 Stress distribution with various crack angles for Mode I fracture	32
3.20 Mode I fracture toughness for various crack angles with respect to the principal material direction	32
3.21 Stress distribution for various angled cracks under Mode II fracture.....	33
3.22 Mode II fracture toughness for various crack angles with respect to the principal material direction	33
4.1 SENB specimen geometry	36
4.2 Four-point bending test setup on a material testing machine	37
4.3 Load-displacement curves of four-point bending tests on carbon foam.....	37
4.4 Unit cell of solid model.....	38
4.5 Boundary conditions on the unit-cell surfaces and maximum principal stress distribution when the unit-cell is stretched in the y -direction.....	41
4.6 Boundary conditions on the unit-cell surfaces and maximum principal stress distribution when the unit-cell is stretched in the y -direction.....	41
4.7 Elastic modulus E^* as a function of relative density (solidity) for $E_s = 2.6$ GPa.	42
4.8 Shear modulus G^* as a function of relative density (solidity) for $E_s = 2.6$ GPa.	42
4.9 Unit cell of beam model.....	43

4.10 Maximum principal stress distribution of solid and beam models for a unit K_I at the crack tip.....	45
4.11 Variation of fracture toughness of carbon foam with relative density.....	46
A.1 Unit cell of solid model.....	50
B.1 Polar coordinate oriented from crack tip.....	54

Abstract of Thesis Presented to the Graduate School
of the University of Florida in Partial Fulfillment of the
Requirements for the Degree of Master of Science

**A MICROMECHANICS METHOD TO PREDICT
THE FRACTURE TOUGHNESS OF CELLULAR MATERIALS**

By

Sukjoo Choi

December 2002

Chairman: Dr. Bhavani V. Sankar

Major Department: Mechanical and Aerospace Engineering

Cellular materials, such as carbon foam, are ideal core materials for sandwich composites in many applications because of their thermal resistance, low density, impact damage tolerance and cost effectiveness. Moreover, carbon foam is a good material for heat exchangers and thermal protection systems.

The Mode I, Mode II and mixed mode fracture toughness of a cellular medium is predicted by simulating the crack propagation using a finite element model. For the sake of simplicity, the cellular medium is considered as a rectangular open cell structure, and the struts are assumed to be beams of square cross section. On the macro-scale, the cellular solid is considered as an orthotropic material. A crack parallel to one of the principal material directions is assumed to exist in the solid and a small region surrounding the crack tip is modeled using beam finite elements. Displacements are imposed on the boundary of the region such that the crack tip is subjected to a given stress intensity factor for orthotropic materials. The struts are assumed to fail in a brittle

manner when the maximum tensile stress becomes equal to the strength of the strut material, and the corresponding stress intensity factor is taken as the fracture toughness of the cellular medium. Based on the finite element results a semi-empirical formula is also derived to predict the Mode I and Mode II fracture toughness of cellular solids as a function of relative density. Results are also presented for mixed mode fracture, and a simple mixed mode fracture criterion is derived for cellular solids. It is found that the fracture toughness is a strong function of the relative density, but the cell size also has a significant effect. Cracks inclined to the principal material directions were also considered, and the Mode I and Mode II fracture toughness was calculated as a function of the crack inclination angle.

Fracture toughness of carbon foam was estimated by experimental analysis and also finite element method. Mode I fracture toughness of open cell carbon foam was measured using single edge notched four-point bend specimens. A micromechanical model was developed assuming a rectangular prism as the unit-cell. The cell walls were modeled using three-dimensional solid element. Aforementioned finite element micromechanical analysis was performed to predict the fracture. The micromechanical simulations were used to study the variation of fracture toughness as a function of relative density of the foam. The good agreement between the finite element and experimental results for fracture toughness indicates that micro-mechanics can be an effective tool to study crack propagation in cellular solids.

CHAPTER 1 INTRODUCTION

Cellular materials are made up of a net work of beam or plate structures leaving an open space or cell in between. Cellular materials, e.g., carbon and polymeric foams, offer several advantages of thermal resistance, durability, low density, impact damage tolerance and cost effectiveness. They have great potential as core materials for sandwich construction, heat exchangers and thermal protection systems in the military and commercial aerospace structures.

An excellent treatise on the structure and properties of cellular solids has been written by Gibson and Ashby [1]. While analytical methods of thermal and mechanical properties of carbon foam are well documented, research on fracture behavior of various foams is still in its infancy. Gibson and Ashby [1] have presented approximate formulas for Mode I fracture toughness of cellular solids in terms of their relative density and tensile strength. These are limited to cracks parallel to the principal material direction. Also, fracture behavior under mixed mode was not studied.

A SEM was used to capture the images of carbon foam as shown in Figure 1.1. In microscopic observation, the open-cell foams are irregularly sized and spaced. For high-density carbon foam (300 to 800 kg/m^3), the length of cell edges is in the range of $1,000 \mu\text{m}$ to $2,000 \mu\text{m}$. For low-density carbon foam (160 to 300 kg/m^3), the cell length is in the range of $200 \mu\text{m}$ to $600 \mu\text{m}$.

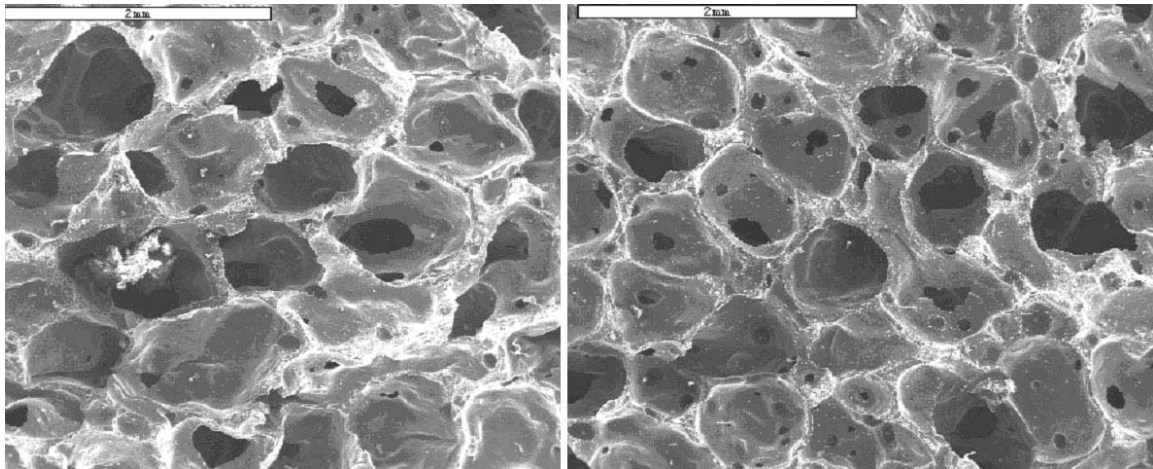


Figure 1.1 SEM images of low (left) and high (right) density carbon foam

The geometry of the foam is categorized by tetrakaidecahedra cells containing 14 faces, 36 edges and 24 vertices as depicted in Figure 1.2.

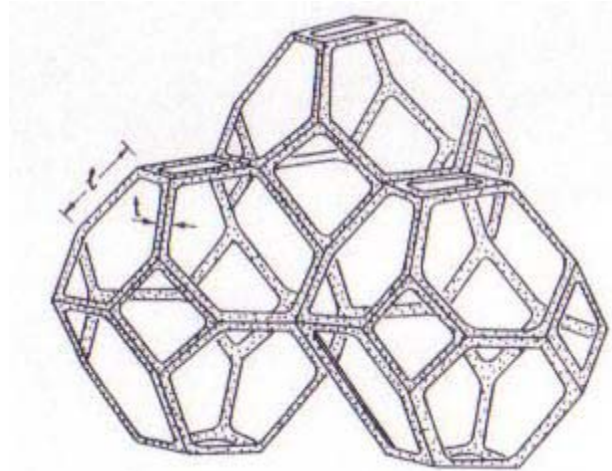


Figure 1.2 The packing of polyhedra to fill space: tetrakaidecahedra

In this study, finite element models are used to predict the fracture toughness of some cellular media under mixed mode conditions. Based on the microscopic observation of carbon foam in Figure 1.1, both cracks parallel to principal material direction and angled crack are considered. For the sake of simplicity, the cellular medium is considered as a rectangular open cell structure, and the struts are assumed to be beams of square cross section of a side h as shown in Figure 1.3.

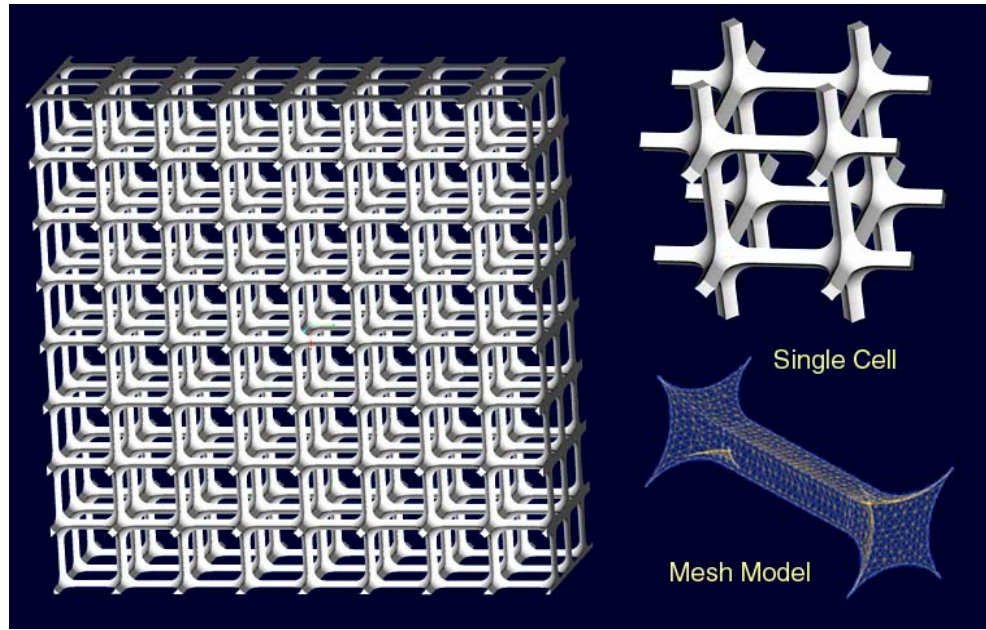


Figure 1.3 Open rectangular cell model

On the macro-scale level, the cellular solid is considered as an orthotropic material. A crack parallel to one of the principal material directions is assumed to exist in the solid and a small region surrounding the crack tip is modeled using beam finite elements. For carbon foam, material properties of cellular structure are referred from pure carbon. Therefore, the Zoltex Panes 30MF High Purity Hilled carbon fiber (Table 1.1) is chosen because of the high percentage of carbon component weight (99.5%).

Table 1.1 Material properties of the Zoltex carbon fiber

Density	1750 kg/m ³
Modulus of Elasticity	207 Gpa
Poisson Ratio	0.17
Ultimate Tensile Strength	3600 Mpa

CHAPTER 2

ELASTIC CONSTANTS OF THE FOAM

In order to estimate the Young's modulus E_1 in the principal material direction we subject the foam to a uniform macro-stress σ^* in the 1 direction (see Figure 2-1) where superscript of * describes the macromechanics properties and the subscript of s is micromechanics properties.

Formulation of Micro-Mechanics Properties

The total tensile force acting on a strut is given by $F = c^2 \cdot \sigma^*$, where c is the length of the unit cell. The micro-stress (actual stress) in the strut can be derived as

$$\sigma_s = \frac{F}{A} = \frac{c^2 \sigma^*}{h^2} \quad (2.1)$$

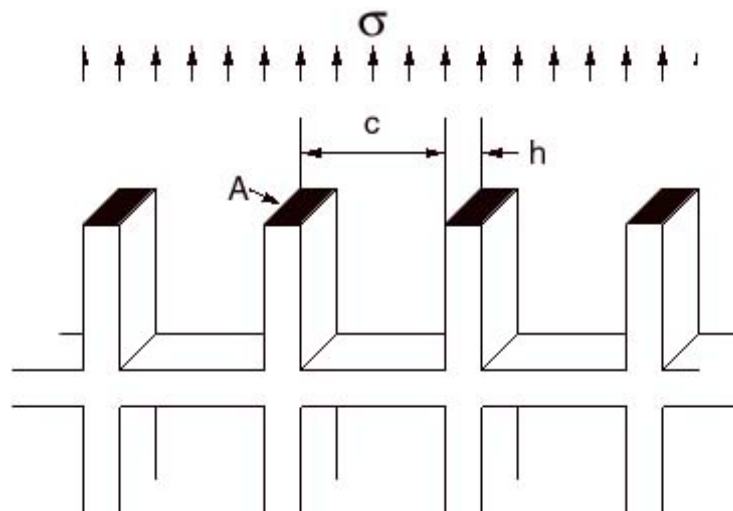


Figure 2.1 Applied stress for a open-cell foam

where h is the cross sectional dimension of the square strut. It should be noted that both the macro-strain ε^* and micro-strain ε are assumed to be equal. The micro-strain is given by

$$\varepsilon_s = \frac{\sigma_s}{E_s} \quad (2.2)$$

Substituting for σ_s from Eq. (2.1) into Eq. (2.2) we obtain

$$\varepsilon_s = \frac{\sigma_s}{E_s} = \frac{\frac{c^2 \sigma^*}{h^2}}{E_s} = \frac{c^2 \sigma^*}{h^2 E_s} = \varepsilon^* \quad (2.3)$$

where E_s is elastic modulus of the strut material. The Young's modulus of the foam can be obtained from Eq. (2.3) as

$$E^* = \frac{\sigma^*}{\varepsilon^*} = \frac{\sigma^*}{\frac{c^2 \sigma^*}{h^2 E_s}} = \left(\frac{h}{c} \right)^2 E_s \quad (2.4)$$

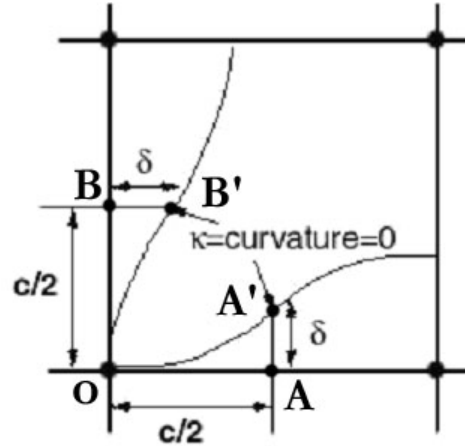


Figure 2.2 Deformed shape of struts on open-cell foam

To calculate the shear modulus G_{12} , the unit-cell is subjected to a state of uniform shear as shown in Figure 2.2. The deformed shape of the struts is shown in thin lines. Due to anti-symmetry the curvature of the deformed beam at the center of the strut must be

equal to zero and hence the bending moment at the center of the strut must also be equal to zero [2]. This fact can be used to find a relation between F and M as $M=Fc/2$. Now half-of the strut, either OA or OB, can be considered as a cantilever beam subjected to a tip force F . The transverse deflection is given by

$$\delta = \frac{F\left(\frac{c}{2}\right)^3}{3E_s I} \quad (2.5)$$

where I , the moment of inertia of the strut cross section is given by $I = \frac{h^4}{12}$.

The macroscopic shear stress τ^* is related to the shear force F as

$$\tau^* = \frac{F}{c^2} \quad (2.6)$$

The macroscopic shear strain γ^* can be calculated as

$$\gamma = \frac{2\delta}{c} = \frac{4\delta}{2} \quad (2.7)$$

The shear modulus of the foam G_{12}^* is defined as the ratio of the macroscopic shear stress τ^* and macro-shear strain γ^* . Then from Eq. (2.6) and Eq. (2.7) we obtain

$$G_{12}^* = \frac{\tau^*}{\gamma^*} = \frac{1}{2} E_s \frac{h^4}{c^4} \quad (2.8)$$

From the expressions for E_1^* and G_{12}^* a relationship between the shear modulus and the Young's modulus can be derived as

$$\frac{E^*}{G^*} = \frac{E_s \frac{h^2}{c^2}}{\frac{1}{2} E_s \frac{h^4}{c^4}} = 2 \frac{c^2}{h^2} \quad (2.9)$$

Due to the symmetry of the structure it is obvious that $E_2=E_3=E_1$ and $G_{23}=G_{31}=G_{12}$.

Further, since we are using beam theory to model the struts, all the Poisson's ratios referred to the principal material directions, ν_{12} , ν_{23} , and ν_{31} are equal to zero.

The relative density ρ^*/ρ_s , where ρ_s is the solid density or the density of the strut material, is a measure of solidity of the cellular material. The density of the foam can be obtained from the mass m and volume V of the unit-cell as shown below:

$$\frac{\rho^*}{\rho_s} = \frac{m}{V} = \frac{\frac{\rho_s(3h^2c - 2h^3)}{c^3}}{\rho_s} = \frac{(3h^2c - 2h^3)}{c^3} = 3\left(\frac{h}{c}\right)^2 - 2\frac{h^3}{c^3} \quad (2.10)$$

If the aspect ratio of the strut $h/c \ll 1$, the relative density can be approximated as

$$\frac{\rho^*}{\rho_s} = 3\left(\frac{h}{c}\right)^2 - 2\frac{h^3}{c^3} \approx 3\left(\frac{h}{c}\right)^2 \quad (2.11)$$

Finite Element Verification of Analytical Models

A portion near the crack tip of the foam was modeled using finite elements. Each strut was modeled as an Euler-Bernoulli beam. Each beam element has 3 integration points. Although we could have one unit-cell with periodic boundary conditions by Marrey and Sankar [2], a larger portion of the cellular medium was modeled as the computational cost is not very high for this case. The model shown in Figure 2.3 consists of 100×100 cells. The cell length c of the unit-cell is $200 \mu\text{m}$ and the strut is assumed to have a square cross section with a side equal to $20 \mu\text{m}$. A uniform displacement ($\delta_2 = 0.01 \text{ m}$) is applied at nodes on the top edge of the model. The total force in the 2 direction is computed from the FE results. The average tensile stress (macro-stress σ_2) can be obtained by

$$\sigma_2^* = \frac{\sum F_y}{L c} \quad (2.12)$$

where the Σ sign denotes summation of all nodal forces and L is the width of the foam considered in the FE model (see Figure 2.3).

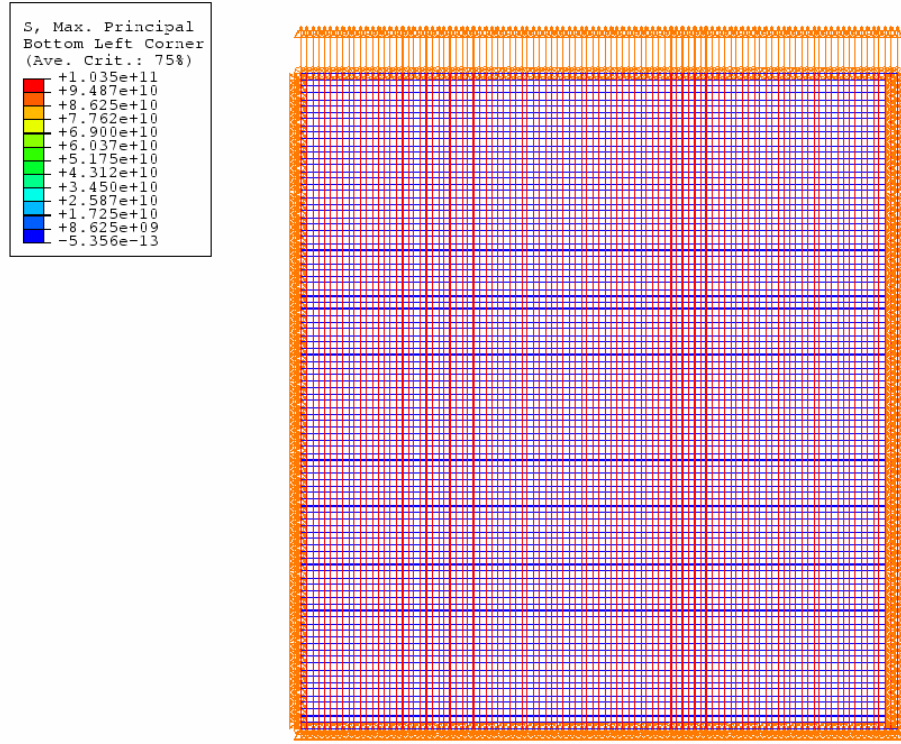


Figure 2.3 Stress distribution of tensile loading on open-cell foam

The Young's modulus E_2^* of a foam can be determined by the stress-strain definition as

$$E_1^* = \frac{\sigma^*}{\varepsilon^*} = \frac{\frac{\sum F_y}{L c}}{\frac{\delta}{L}} = \frac{\sum F_y}{c \delta} \quad (2.13)$$

For the case considered the FE model gave a value $E_1^* = 2.09$ GPa and the analytical model Eq. (2.4) yielded a value of 2.07 GPa. The difference of results is 1%.

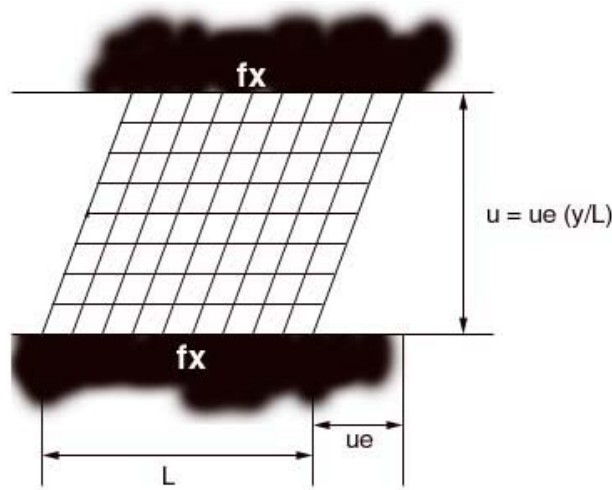


Figure 2.4 Shear applied on open-cell foam

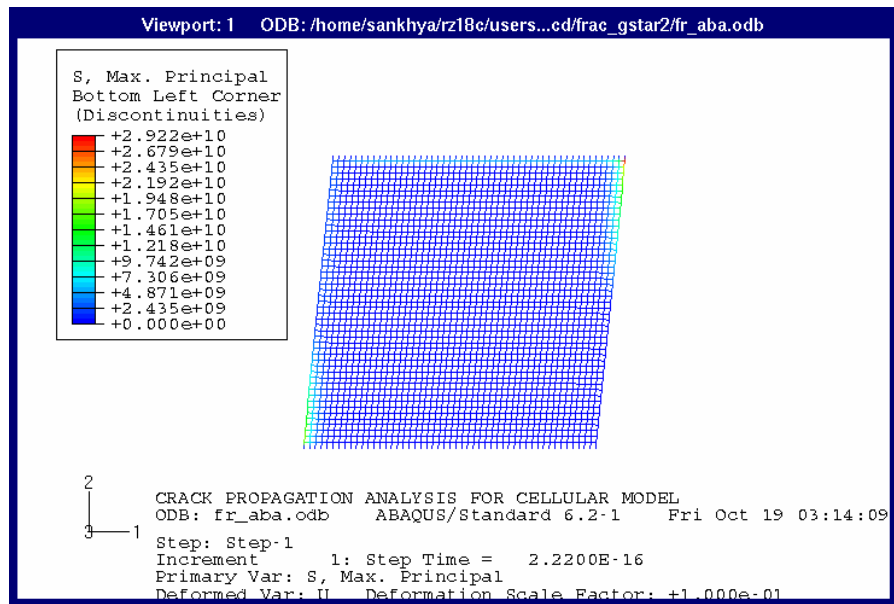


Figure 2.5 Stress distribution of shear loading on open-cell foam

To estimate the shear modulus by numerical analysis, a constant horizontal displacement u_s is applied to all the nodes on the topside of the foam as shown in Figure 2.4. The shear stress τ^* can be obtained by the sum of reaction forces F divided by the area of the top surface:

$$\tau^* = \frac{\sum F_x}{Lc} \quad (2.14)$$

where L is the length of the foam considered in the FE model and c is the unit-cell dimension. The shear strain γ^* can be calculated as

$$\gamma = \frac{u_s}{L} \quad (2.15)$$

Thus, shear modulus G_{12}^* of the foam can be estimated as

$$G^* = \frac{\tau^*}{\gamma} = \frac{\frac{\sum F_x}{L c}}{\frac{u_s}{L}} = \frac{\sum F_x}{u_s c} \quad (2.16)$$

The deformed shape of the cellular solid under shear is shown in Figure 2.5. From the FE model the shear modulus of the foam was estimated as 10.25 MPa, whereas the aforementioned analytical model Eq. (2.8) yields 10.35 MPa. The difference between the two results is about 1%. The FE model is slightly compliant because of lack of constraints on the side and applying periodic boundary conditions would have yielded values closer to the analytical solution.

CHAPTER 3

FINITE ELEMENT METHODS OF FRACTURE TOUGHNESS

In this section, we describe a finite element based micromechanics model for estimating the fracture toughness of the cellular solid. The crack is assumed to be parallel to one of the principal material axes, and Mode I, Mode II and mixed mode fracture are considered. To determine the fracture toughness a small region around the crack tip is modeled using beam elements. A constant mode mixity K_I/K_{II} is assumed to be applied. The boundary of the cellular solid is subjected to displacement (u_1 and u_2) boundary conditions corresponding to an arbitrary value of K_I (or K_{II}). The rotational degree of freedom at each node of the beam element on the boundary of the solid is left as unknown and no couples are applied at these nodes. The calculation of boundary displacements for a given stress intensity factor is described in the next section.

Boundary Displacement at a Crack Tip

The displacement components in the vicinity of a crack tip in a homogenous orthotropic material are derived in Appendix B and they are as follows:

Displacement field for Mode I:

$$\begin{aligned} u_x &= K_I \sqrt{\frac{2r}{\pi}} \operatorname{Re} \left\{ \frac{1}{s_1 - s_2} \left[s_1 p_2 (\cos \theta + s_2 \sin \theta)^{1/2} - s_2 p_1 (\cos \theta + s_1 \sin \theta)^{1/2} \right] \right\} \\ u_y &= K_I \sqrt{\frac{2r}{\pi}} \operatorname{Re} \left\{ \frac{1}{s_1 - s_2} \left[s_1 q_2 (\cos \theta + s_2 \sin \theta)^{1/2} - s_2 q_1 (\cos \theta + s_1 \sin \theta)^{1/2} \right] \right\} \end{aligned} \quad (3.1)$$

Displacement field for Mode II:

$$\begin{aligned} u_x &= K_{II} \sqrt{\frac{2r}{\pi}} \operatorname{Re} \left\{ \frac{1}{s_1 - s_2} \left[p_2 (\cos \theta + s_2 \sin \theta)^{1/2} - p_1 (\cos \theta + s_1 \sin \theta)^{1/2} \right] \right\} \\ u_y &= K_{II} \sqrt{\frac{2r}{\pi}} \operatorname{Re} \left\{ \frac{1}{s_1 - s_2} \left[q_2 (\cos \theta + s_2 \sin \theta)^{1/2} - q_1 (\cos \theta + s_1 \sin \theta)^{1/2} \right] \right\} \end{aligned} \quad (3.2)$$

In deriving the above expressions, the crack is assumed to be parallel to the x axis, and $r-\theta$ is the polar coordinate system oriented at the crack tip. The complex parameters p , q , and s depend on the elastic constants of the homogeneous orthotropic material as described in the Appendix B.

Model Setup

The commercial FE program ABAQUS is used to conduct numerical analysis. A FE model of open cell foam is taken around the small portion of the crack tip in Figure 3.1. The boundary condition of small portion is determined by using the solution for boundary displacements in the previous section. A crack in the FE model is created by removing beam elements.

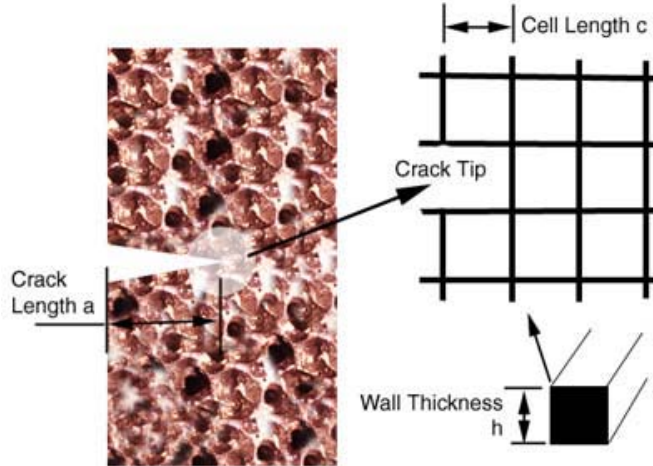


Figure 3.1 Open-cell foam model with a crack

To reduce the modeling cost, a FORTRAN code was written to generate nodal and element properties with user specified unit-cell configuration. The code calculates

boundary displacements at corresponding boundary nodal coordinates. After execution, it exports an ABAQUS input file so that the ABAQUS can read the input directly.

The maximum tensile stress in the struts is calculated from the finite element method. The FE analysis outputs axial force, bending moment and shear force at each node of the beam elements, and the maximum tensile stress was calculated using a separate program. Usually the maximum stress occurs at the crack tip strut. From the result the value of K_I (or K_{II}) that will cause rupture of the strut is estimated, which then is taken as the fracture toughness of the cellular solid.

Before we describe an analytical model for estimating the fracture toughness, we will discuss the results from the FE simulation. At first, we will check the validity of applying continuum fracture mechanics. It was found that a model consisting of 100×100 cells (total 10,000 cells) gave a converged result for fracture toughness and the same model is used throughout the study. The run time for this model is about 13½ minutes in a 1.7 GHz Intel Pentium 4 computer.

Convergence Analysis for Mode I

The convergence analysis is performed to evaluate variation of fracture toughness with various sizes of foam models, 1.2cm × 1.2cm (3,600 cells), 2cm × 2cm (10,000 cells), 4cm × 4cm (40,000 cells) and 8cm × 8cm (160,000 cells). The foam model properties are shown in Table 3.1.

Table. 3.1 Foam model properties for convergence analysis

Length of cell edge	200 μm
Cell wall thickness	20 μm
Relative density	0.0280
Tensile strength	3600Mpa

As the model size increases, fracture toughness becomes stable at approximately 4.67×10^5 Pa m^{1/2} in Figure 3.2. For a foam model containing from 10,000 to 160,000 cells, variation in fracture toughness is 2.7%. Therefore, the 10,000 cell model is chosen for further numerical analysis to maintain output accuracy with less CPU time. For the 10,000 cell model, a computer with 1.7GHz Intel Pentium 4 takes 13½ minutes to complete the job, but the 160,000 cells takes 2 hours more.

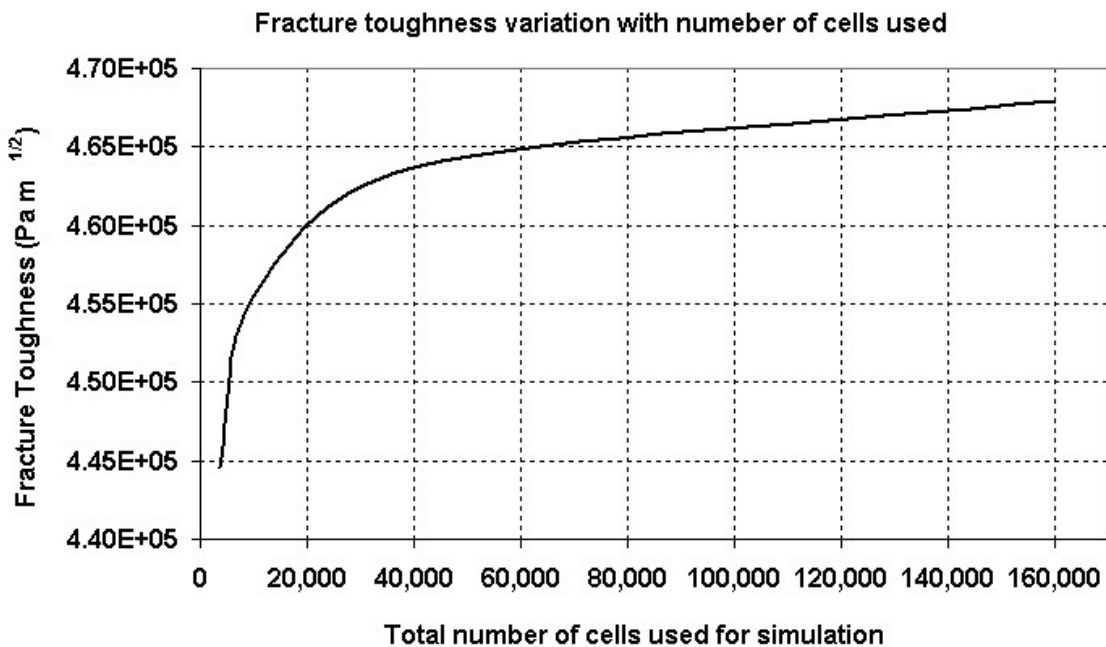


Figure 3.2 Variation of fracture toughness with various model sizes

The axial stress along the crack path from a crack tip is shown in Figure 3.3. In the result, smaller models produce higher axial stress at the crack tip. Further from the crack tip, variation in axial stresses becomes insignificant for all model sizes.

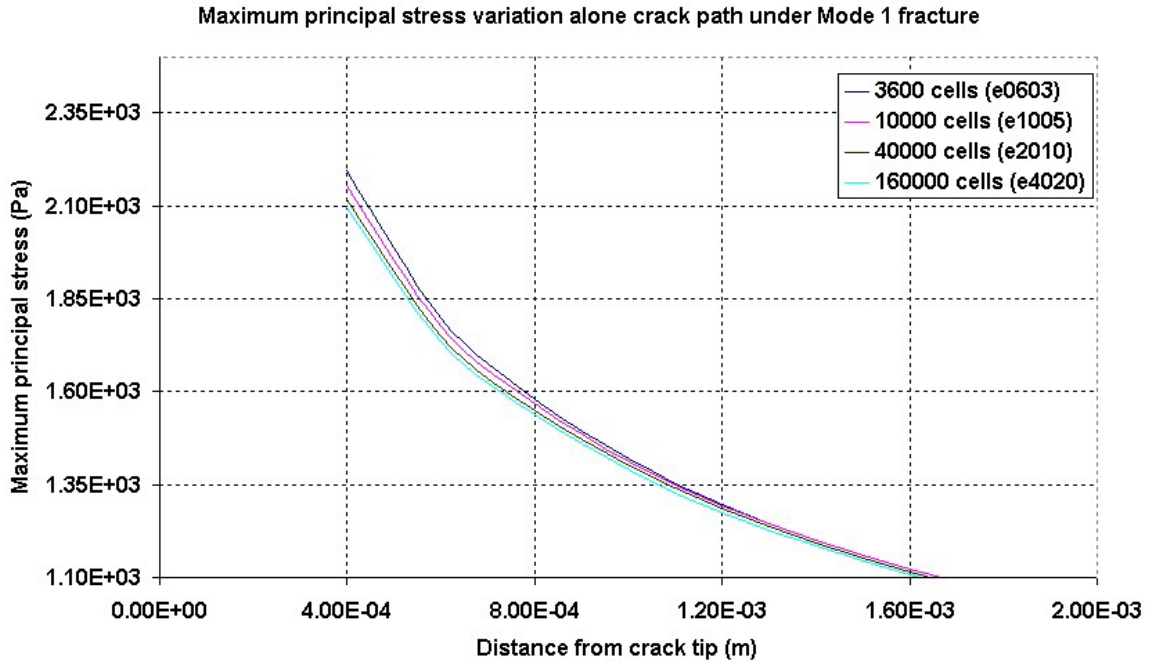


Figure 3.3 Axial stress variation from a crack tip for various model sizes

The log-log plot of maximum strut stress variation from the crack tip is shown in Figure 3.3, the curve is fitted to the equation

$$\sigma = \frac{41.69}{\sqrt{r}} \quad (3.3)$$

Using the relation between micro and macro stresses in Eq. (2.1), Eq. 3.4 can be written as

$$\sigma^* = \frac{1.05}{\sqrt{2\pi r}} \quad (3.4)$$

indicating that the macro stress in tensile factor is equal to 1.05 which is approximately equal to the applied the stress intensity factor K_I of unity.

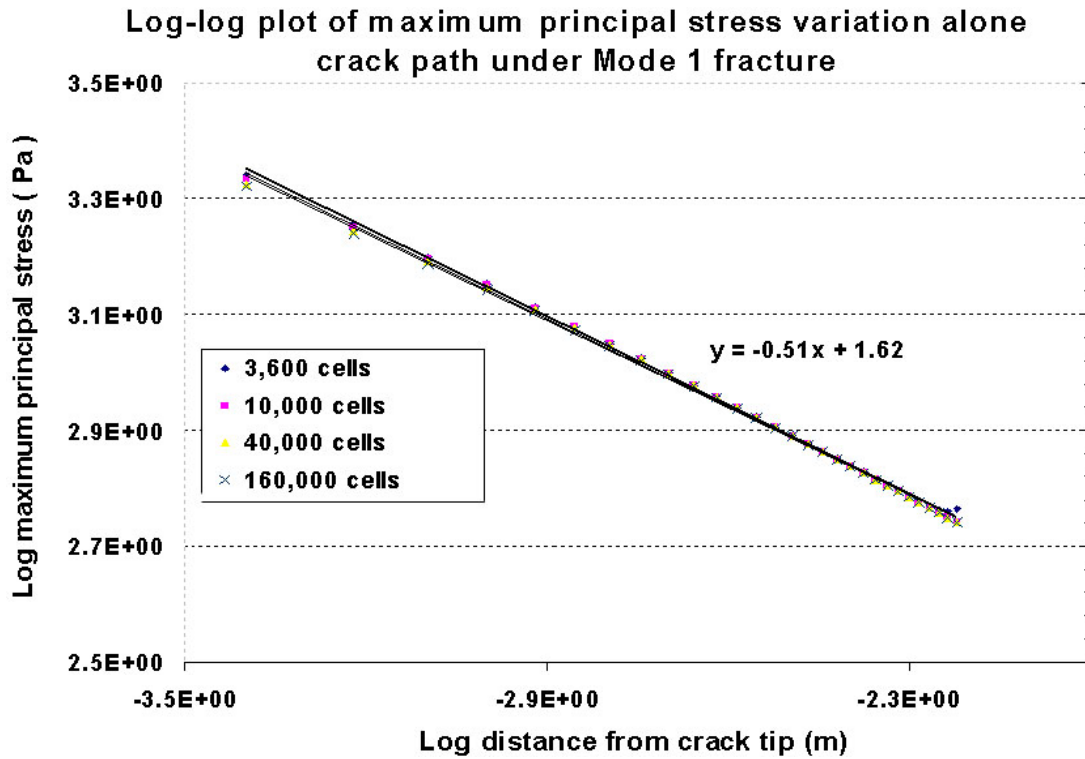


Figure 3.4 Log-log plot of axial stress along a crack tip for various model sizes

If the fracture toughness estimated by using the present method is truly a material(macrosopic) property, then it should be independent of the crack length. Hence the crack length was varied in the micromechanical method. The results are shown in Figure 3.5. The predicted fracture toughness was plotted as a function of percentage of crack length in the model. The results clearly show that idea of modeling the foam as a homogenous material is quite acceptable.

Variation of Crack Length on Mode I fracture

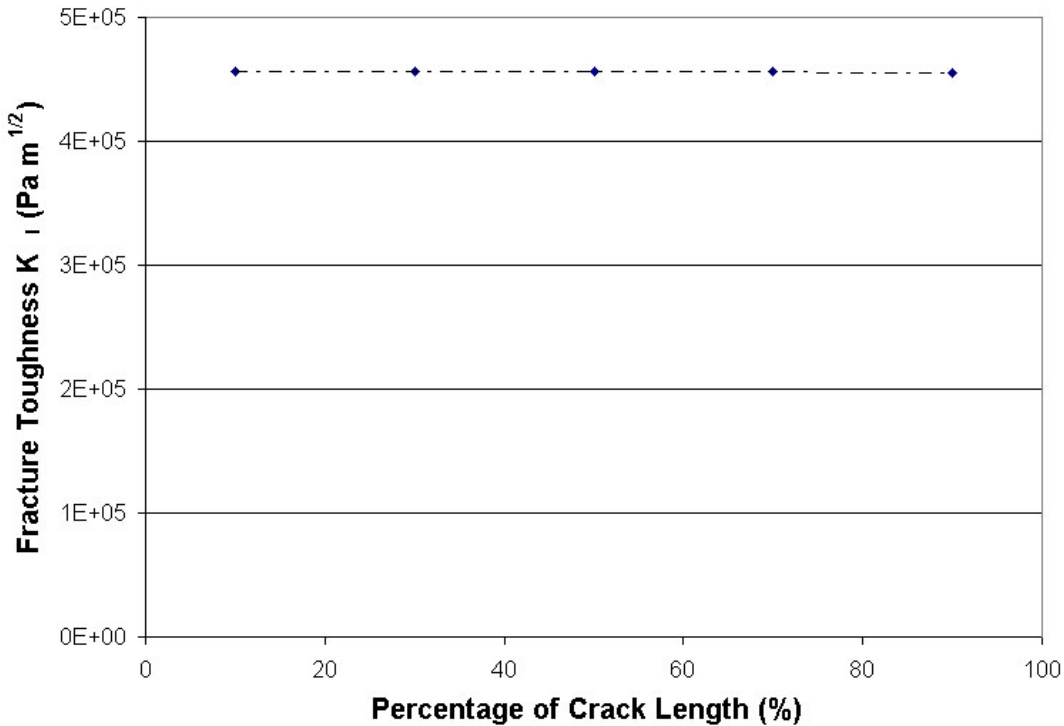


Figure 3.5 Fracture toughness in various crack lengths

Mode I Fracture Toughness of Open Cell Foam

Since the relative density depends on the length of the strut c and a cell wall thickness h , the fracture simulation is conducted in two cases. In the first case, c is varied and h is kept constant. The second case, h varied while c is constant.

The results of the FE simulation are axial force, bending moment and shear force in each element, which are used to calculate the maximum principal stress at the crack tip, and then the fracture toughness. A sample stress distribution due to Mode I fracture is shown in Figure 3.6.

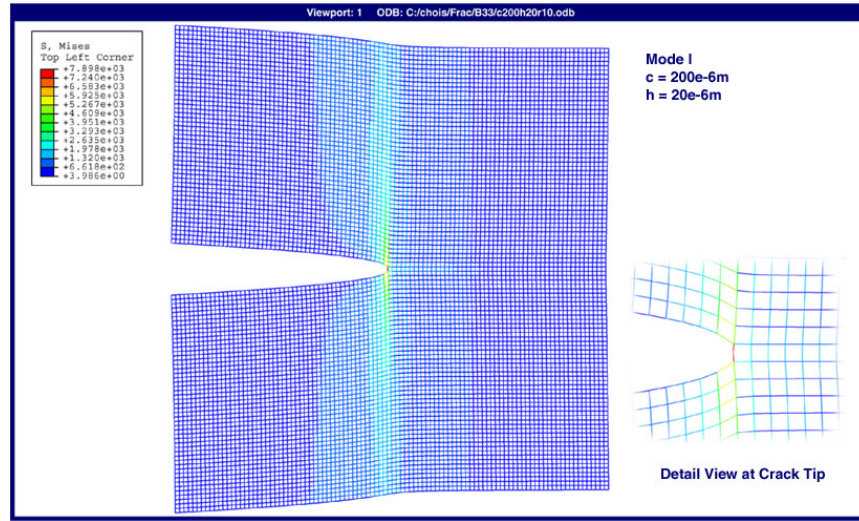


Figure 3.6 Stress distribution of Mode I fracture ($c=200 \mu\text{m}$, $h=20 \mu\text{m}$)

The variation of fracture toughness with relative density is shown in Figure 3.7.

The results of fracture toughness in Figure 3.7 are fitted to a curve with a power of 1.045 for constant wall thickness and 0.7879 for constant length of strut. To obtain a higher fracture toughness, increasing cell wall thickness h is more effective while cell length c is constant.

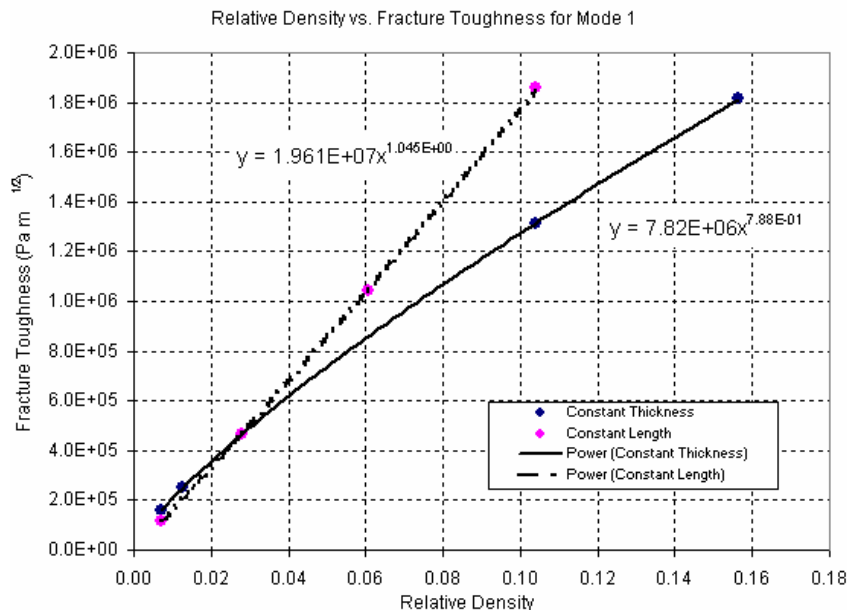


Figure 3.7 Mode I fracture toughness for two cases

Mode II Fracture Toughness of Open Cell Foam

The analysis of Mode II fracture toughness is performed in same manner as the Mode I fracture analysis in previous section. Unlike to Mode I fracture, the boundary displacements are not symmetric about the crack plane as shown in Figure 3.8.

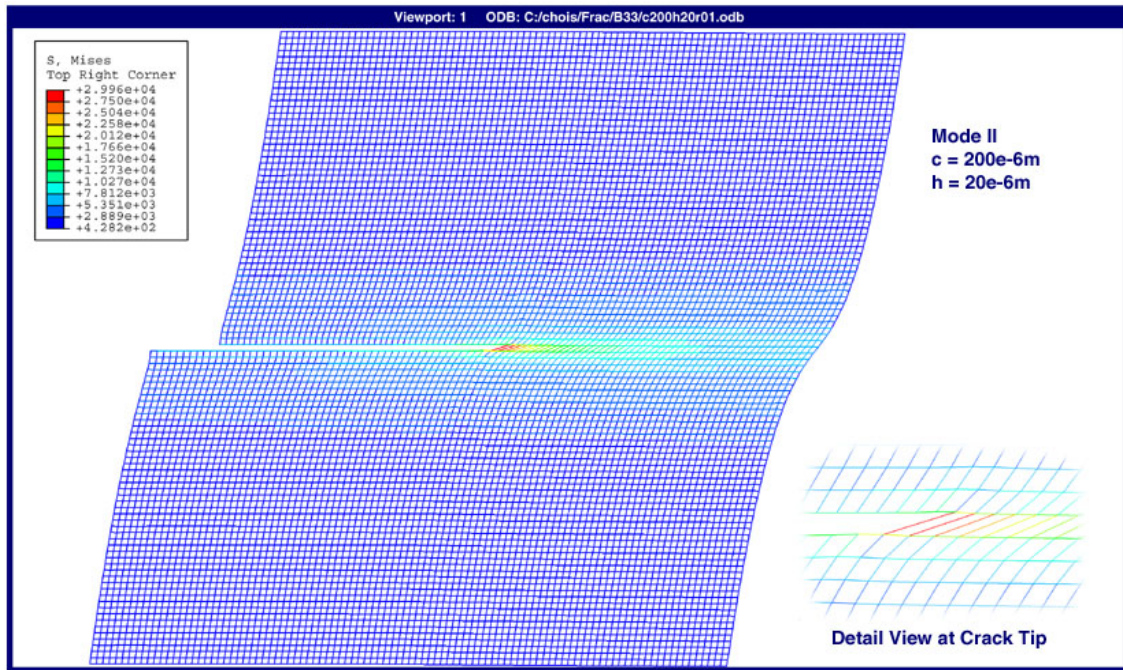


Figure 3.8 Stress distribution of Mode II fracture ($c=200\mu\text{m}$, $h=20\mu\text{m}$)

The results of Mode II fracture toughness are fitted in a curve with power of 1.0654 for constant wall thickness h and 1.3231 for the constant cell length c in Figure 3.9. Therefore, to obtain the higher fracture toughness, increasing cell wall thickness h is more effective than increasing cell length c for Mode II.

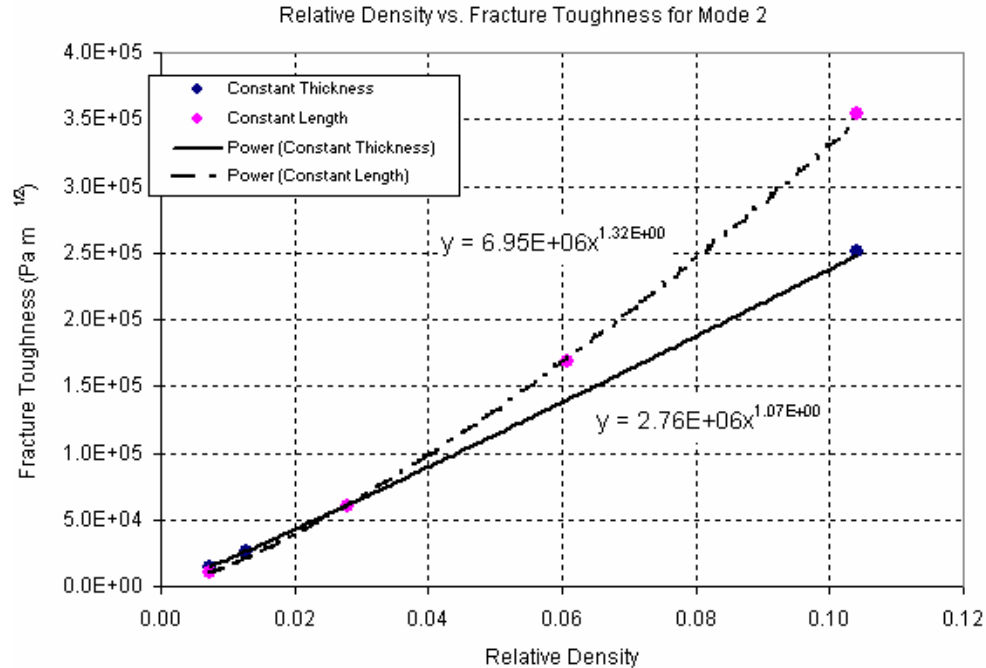


Figure 3.9 Numerical result of fracture toughness for Mode II

Fracture Toughness of Mixed Mode on Open Cell Foam

For the mixed mode fracture analysis, the boundary displacements for Mode I and Mode II are superposed for various ratios of Mode I and Mode II in Figure 3.10. A sample deformation under mixed mode is shown in Figure 3.10.

Fracture toughness for mixed mode is shown for constant length of cell edge in Figure 3.11 and constant wall thickness in Figure 3.12. The fracture toughness for mixed mode is inversely linearly proportional.

$$\left(\frac{K_I}{K_{IC}}\right)^a + \left(\frac{K_{II}}{K_{IIC}}\right)^b = 1 \quad (3.5)$$

where the constants a and b are 1. The combinations of K_I and K_{II} for fracture are shown in Figure 3.11 for constant cell length and in Figure 3.12 for constant cell wall thickness.

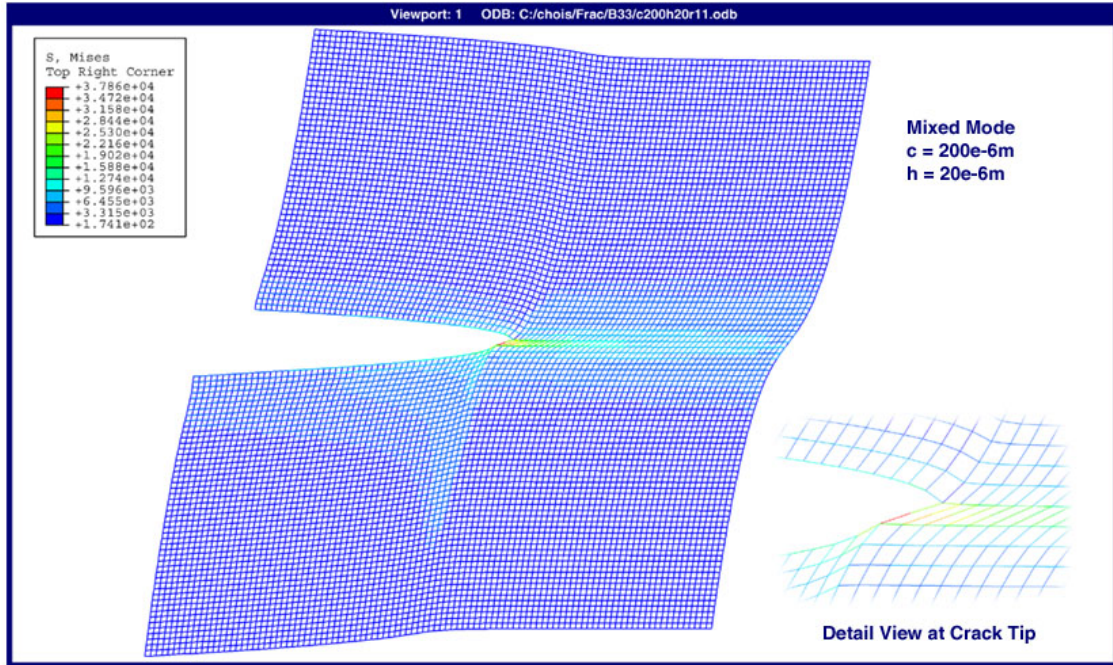


Figure 3.10 Stress distribution on the mixed mode fracture ($c=200\mu\text{m}$, $h=20\mu\text{m}$)

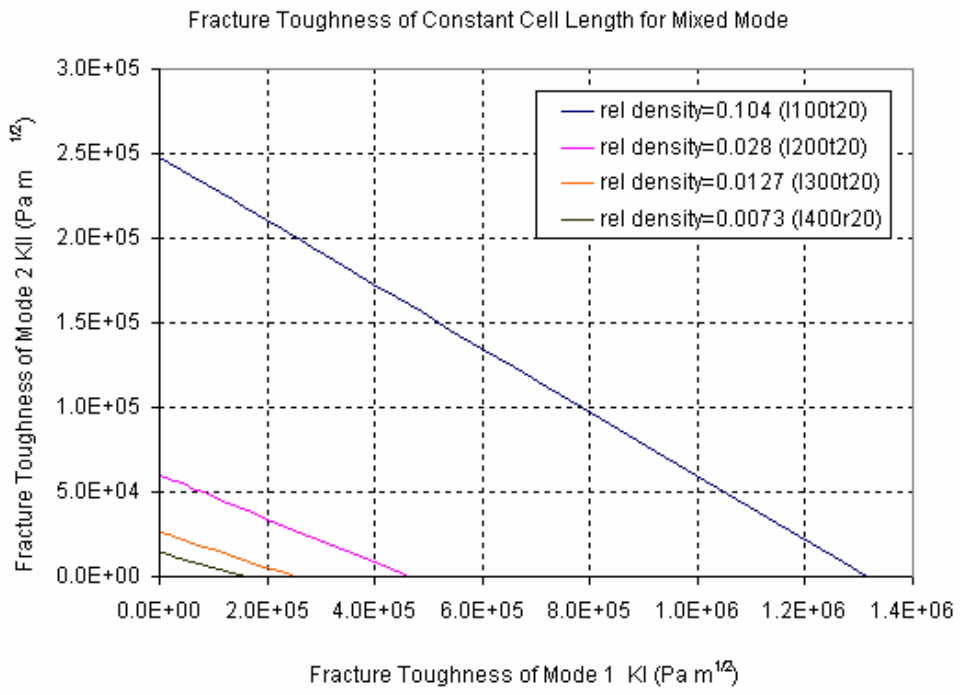


Figure 3.11 Mixed mode fracture toughness of constant length of cell edges

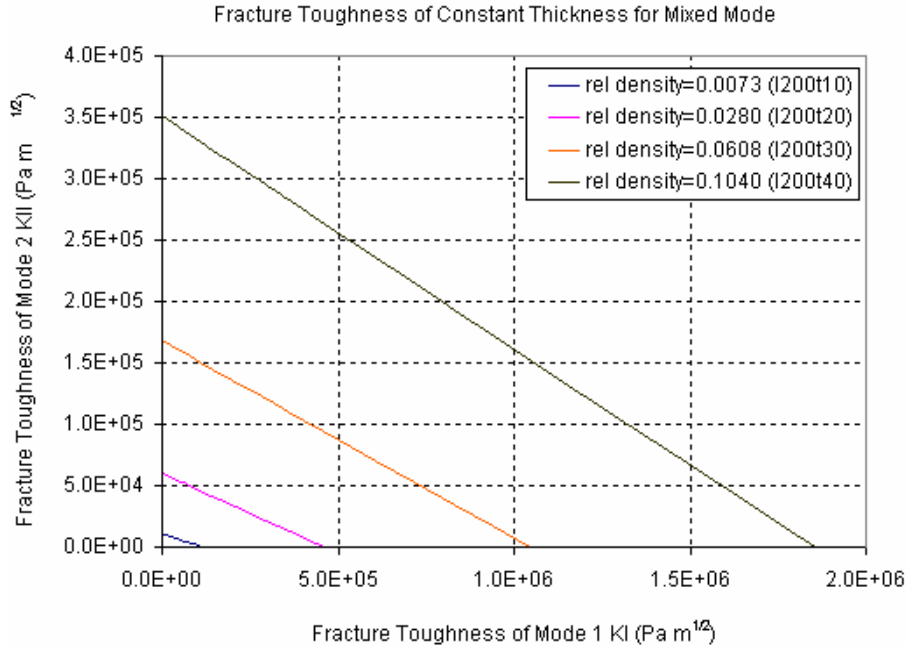


Figure 3.12 Mixed mode fracture toughness of constant cell wall thickness

Formulation of Fracture Toughness for Mode I and Mode II

Analytical Model for Mode I Fracture Toughness

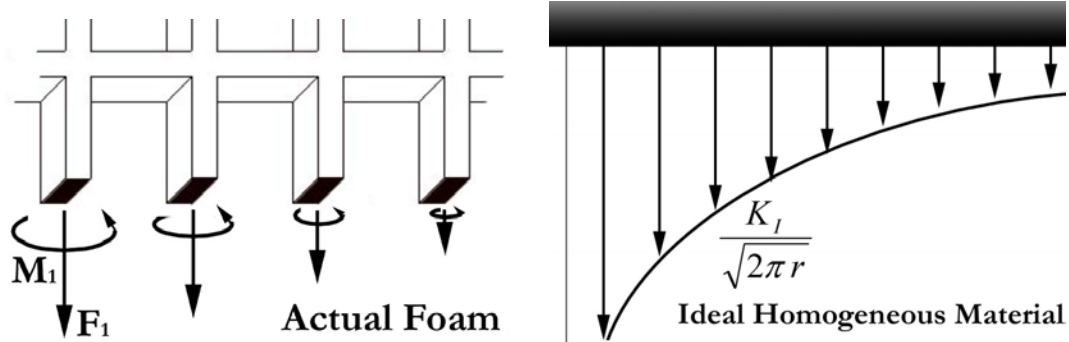


Figure 3.13 Crack tip forces and moments in the actual foam and corresponding crack tip stresses in the idealized homogeneous continuum

In order to derive an analytical model for fracture toughness, the stress intensity factor of the homogeneous model should be related to the actual stresses in the crack tip ligament of the foam. This can be obtained by assuming that the internal forces and bending moment in the crack tip strut are caused by a portion of the crack tip stress field

ahead of the crack tip in the homogeneous model. Let us define a non-dimensional factor α that describes the effective length l as follows:

$$l = \alpha c \quad (3.9)$$

The ideal stress distribution σ_y ahead of crack tip is described as follows:

$$\sigma_y = \frac{K_I}{\sqrt{2\pi r}} \quad (3.10)$$

where r is the distance from the crack tip. The axial force in the crack tip ligament is obtained by integrating the tensile stress σ_y over the effective length

$$F = c \int_0^l \sigma_y dr = K_I \sqrt{\frac{2l}{\pi}} c \quad (3.11)$$

The bending moment M is given by

$$M = c \int_0^l r \sigma_y dr = \frac{K_I c}{\sqrt{2\pi}} \int_0^l \sqrt{r} dr = \frac{K_I c}{\sqrt{2\pi}} \frac{l^{3/2}}{\frac{3}{2}} = K_I \sqrt{\frac{2}{\pi}} \frac{l^{3/2}}{3} c \quad (3.12)$$

Assuming fracture occurs when the maximum bending stress equals the tensile strength of the ligament material, a relationship between the tensile strength and fracture toughness can be derived as

$$\sigma = \frac{My}{I} = \frac{M \frac{h}{2}}{\frac{h^3}{12}} = \frac{6M}{h^3} = \frac{6}{h^3} K_I \sqrt{\frac{2}{\pi}} \frac{l^{3/2}}{3} c = \frac{2\sqrt{2}}{\sqrt{\pi}} K_I \frac{l^{3/2}}{h^3} c \quad (3.13)$$

By substituting for l in terms of α from Eq. (3.9), the fracture toughness can be related to the tensile strength as

$$\sigma = \frac{2\sqrt{2}}{\sqrt{\pi}} K_I \alpha^{3/2} \frac{c^{3/2}}{h^3} c \quad (3.14)$$

Then the fracture toughness of the cellular material can be derived as

$$K_I = \sigma_u \frac{\sqrt{\pi}}{2\sqrt{2}\alpha^{3/2}} \frac{h^3}{c^{5/2}} = \sigma_u \frac{\sqrt{\pi}}{2\sqrt{2}\alpha^{3/2}} \frac{h^2}{c^2} \left(\frac{h}{\sqrt{c}} \right) \quad (3.15)$$

The non-dimensional distance α can be found from the FE results for fracture toughness K_{lc} and the tensile strength of the ligament material as follows:

$$\alpha = \left(\frac{\sigma_u}{K_I} \frac{\sqrt{\pi}}{2\sqrt{2}} \frac{h^3}{c^{5/2}} \right)^{2/3} \quad (3.16)$$

The results for α as a function relative density are plotted in Fig. 3.14. It may be noted that α increases with relative density and the variation can be accurately represented by a power law. Interestingly both constant wall thickness case and the constant spacing case we have studied so far fit accurately into a single power law. The effective crack tip distance is about 10% of the cell spacing for low-density foam and about 305 for high-density foam.

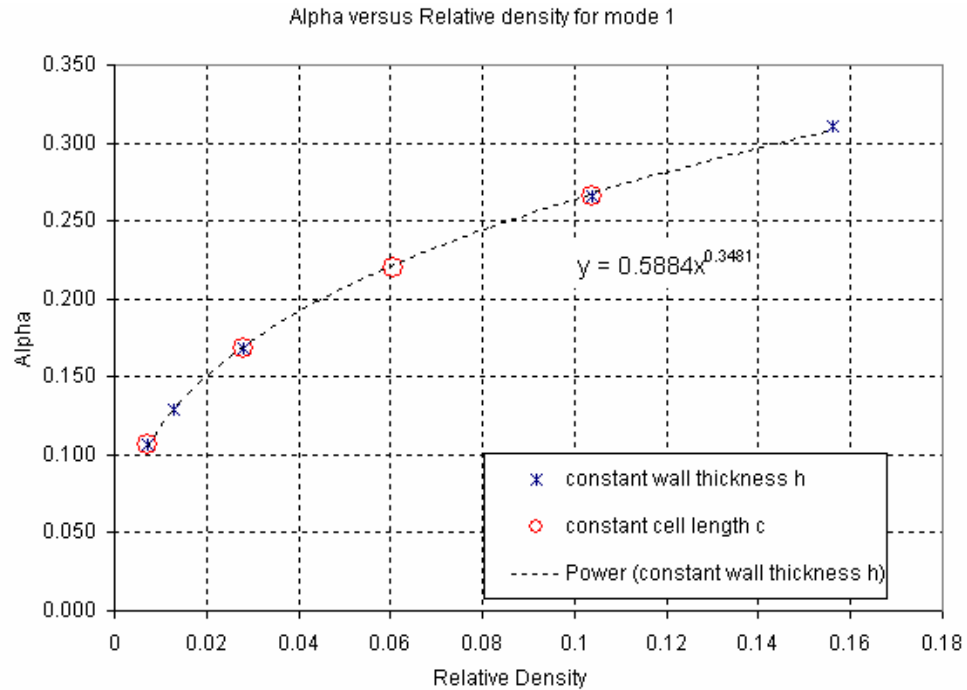


Figure 3.14 Variation of α (l/c) with relative density for Mode I

Analytical Model for Mode II Fracture Toughness

The effective crack tip distance for Mode II can be derived following steps similar to that in the preceding section for Mode I. The shear stress (τ_{xy}) distribution ahead of the crack tip is given by:

$$\tau_{xy} = \frac{K_{II}}{\sqrt{2\pi r}} \quad (3.17)$$

The total shear force F over the effective distance l can be derived as

$$F = c \int_0^l \tau_{xy} dr = K_{II} \sqrt{\frac{2l}{\pi}} c \quad (3.18)$$

The maximum bending moment in the crack tip element is the product of force F and the length $c/2$:

$$M = K_{II} \sqrt{\frac{2l}{\pi}} c \frac{c}{2} \quad (3.19)$$

The maximum bending stress is derived as

$$\sigma = \frac{My}{I} = \frac{M \frac{h}{2}}{\frac{h^3}{12}} = \frac{6M}{h^3} = 3K_{II} \sqrt{\frac{2l}{\pi}} \frac{c^2}{h^3} \quad (3.20)$$

An expression for fracture toughness K_{II} in terms of strut tensile strength, strut dimensions and the effective distance can be derived as

$$K_{II} = \frac{\sigma_u h^3}{3c^2} \sqrt{\frac{\pi}{2l}} \quad (3.21)$$

Since, fracture toughness can be expressed in terms of the non-dimensional distance α :

$$K_{II} = \frac{\sigma_u h^3}{3c^2} \sqrt{\frac{\pi}{2\alpha c}} = \frac{\sigma_u h^3}{3c^{\frac{5}{2}}} \sqrt{\frac{\pi}{2\alpha}} \quad (3.22)$$

From (3.33) an expression for α can be derived as

$$\alpha = \left(\frac{\sigma_u h^3}{3K_{II} c^{\frac{5}{2}}} \sqrt{\frac{\pi}{2}} \right)^2 = \frac{\pi \sigma_u^2 h^6}{18 K_{II}^2 c^5} \quad (3.23)$$

The constant α can be evaluated using the FE results of fracture toughness. The value of α as a function of relative density is plotted in Fig. 3.15. Again, it can be noted that a power law description is adequate for Mode II also. Further the value of α depends only on the relative density and not on individual cell or strut dimensions. The effective distance seems to be slightly less for Mode II. It is about 5% of the strut spacing for low density and about 22% for high density foams.

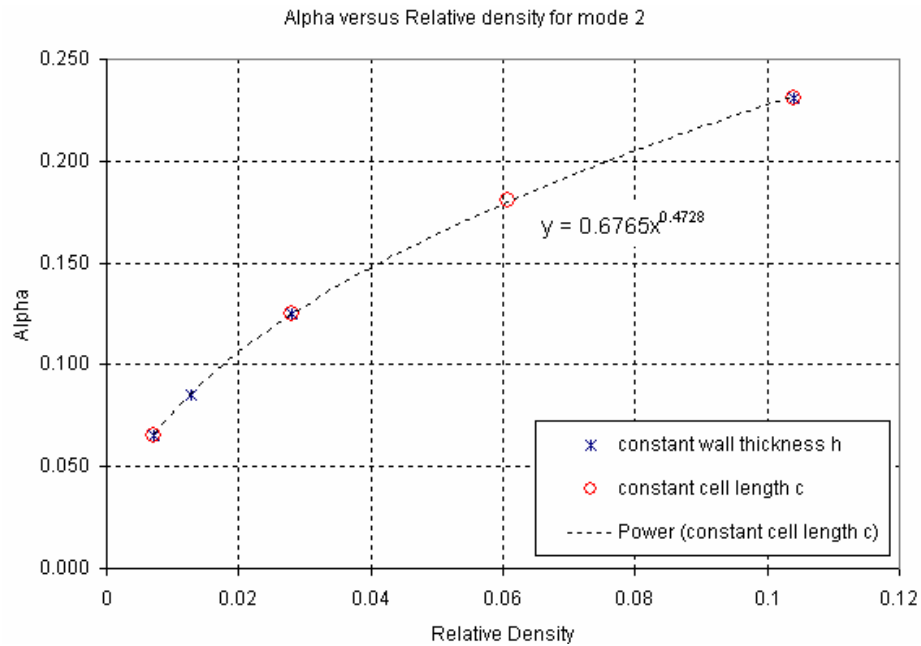


Figure 3.15 Variation of α (l/c) with relative density for Mode II

Mode I and Mode II Fracture Toughness with Angled Crack

So far our attention has been focussed on cracks parallel to the principal material direction. The next step will be to study crack inclined at an angle to the principal direction. Before that, an understanding of how the material will fail under combined

loading will be beneficial. In the following we describe methodologies to predict the failure of the cellular medium under combined loading. The results will then be used to predict the tensile and shear strength in an arbitrary coordinate system.

Prediction of the Maximum Strength under Tensile Loading

When the cellular medium is subjected to combined loading under plane stress conditions, the ligaments in a typical representative volume element will be subjected to axial force, shear force and bending moment as shown in Fig. 3.16.

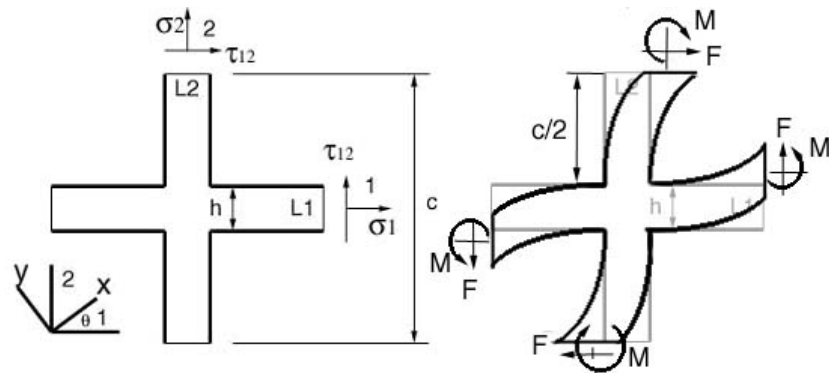


Figure 3.16 Forces in a ligament under combined loading

From the equation (2.1), axial stress can be obtained as

$$\sigma_{axial} = \sigma_1^* \frac{h^2}{c^2} \quad (3.25)$$

The relation between maximum bending moment and the shear force is given by

$$M = F \frac{c}{2} = \tau_{12}^* c^2 \frac{c}{2} = \frac{\tau_{12}^* c^3}{2} \quad (3.26)$$

The maximum stress due to the bending moment can be derived as

$$\sigma_{bending} = \frac{M \bar{y}}{I} = \frac{\frac{\tau_{12}^* c^3}{2} \frac{h}{2}}{\frac{h^4}{12}} = 3 \tau_{12}^* \left(\frac{c}{h} \right)^3 \quad (3.27)$$

It should be noted that we have assumed that only σ_y component of the macro-stress exists. The ligament stresses in Eq. 3.25 and Eq. 3.27 can be expressed in terms of macro-stresses referred to the $x-y$ coordinate system as:

$$\sigma_1^* = \sigma_y^* \sin^2 \theta \quad (3.28a)$$

$$\sigma_2^* = \sigma_y^* \cos^2 \theta \quad (3.28b)$$

$$\tau_{12}^* = -\sigma_y^* \sin \theta \cos \theta \quad (3.28c)$$

Then the micro-stress σ_u under combined loading can be derived as

$$\sigma_{axial} = \sigma_1^* \left(\frac{c}{h} \right)^2 = \sigma_y^* \sin^2 \theta \quad (3.29)$$

$$\sigma_{bending} = 3\tau_{12} \left(\frac{c}{h} \right)^3 = -3\sigma_y^* \sin \theta \cos \theta \quad (3.30)$$

The micro-stress σ_u can be derived as

$$\sigma_u = \sigma_y^* \sin^2 \theta \left(\frac{c}{h} \right)^2 \pm 3\sigma_y^* \sin \theta \cos \theta \frac{c^3}{h^3} = \sigma_y^* \left[\sin^2 \theta \pm 3 \frac{c}{h} \sin \theta \cos \theta \right] \left(\frac{c}{h} \right)^2 \quad (3.31)$$

The maximum stress that can be applied to the cellular medium is obtained by equating the maximum micro-stress to the strength of the ligament material. The ratio of the macro-stress and the micro-stress for ligament L₁ (refer to Fig. 3.16) can be derived as

$$\frac{\sigma_y^*}{\sigma_u} = \frac{1}{\left| \sin^2 \theta \pm 3 \frac{c}{h} \sin \theta \cos \theta \right| \left(\frac{c}{h} \right)^2} \quad (3.32)$$

In the same manner, the ratio of the macro-stress and the micro-stress for ligament L₂ can be derived as

$$\frac{\sigma_y^*}{\sigma_u} = \frac{1}{\left| \cos^2 \theta \pm 3 \frac{c}{h} \sin \theta \cos \theta \left(\frac{c}{h} \right)^2 \right|} \quad (3.33)$$

Eq. (3.32) and Eq. (3.33) are used to calculate the maximum stress σ_y that can be applied to the cellular medium before any ligament failure. Then maximum stress under tensile loading is a function of the orientation θ as shown in Figure 3.17. The strength variation is symmetric about $\theta=45^\circ$.

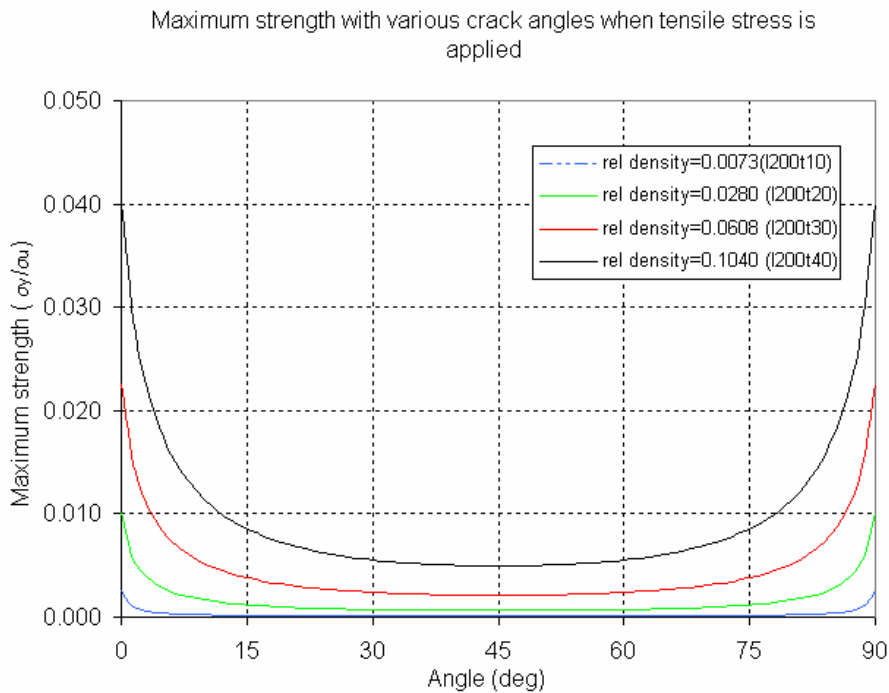


Figure 3.17 Variation of maximum tensile stress σ_y as a function of angle between the xy coordinate system and the principal material directions

Prediction of the Maximum Strength under Shear Loading

The calculation of shear strength at an arbitrary orientation is very similar to that described for tensile strength in the preceding section. The transformation of macro-stresses between the global xy coordinates and the principal material coordinates are given by:

$$\sigma_1^* = \tau_{xy}^* \sin 2\theta \quad (3.34a)$$

$$\sigma_2^* = -\tau_{xy}^* \sin 2\theta \quad (3.34b)$$

$$\tau_{12}^* = \tau_{xy}^* \cos 2\theta \quad (3.35c)$$

It may be noted that only shear component of the macro-stress (τ_{xy}) is present.

Substituting Eq. (3.34) into the Eq. (3.25) and (3.27) we obtain

$$\sigma_{axial} = \sigma_1^* \left(\frac{c}{h} \right)^2 = \tau_{xy}^* \sin 2\theta \left(\frac{c}{h} \right)^2 \quad (3.36)$$

$$\sigma_{bending} = 3\tau_{12}^* \left(\frac{c}{h} \right)^3 = 3\tau_{xy}^* \cos 2\theta \left(\frac{c}{h} \right)^3 \quad (3.37)$$

The micro-stresses can be derived as

$$\sigma_u = \tau_{xy}^* \sin 2\theta \left(\frac{c}{h} \right)^2 \pm 3\tau_{xy}^* \cos 2\theta \left(\frac{c}{h} \right)^3 = \tau_{xy}^* \left[\sin 2\theta \pm 3\frac{c}{h} \cos 2\theta \right] \left(\frac{c}{h} \right)^2 \quad (3.38)$$

The ratio of the macro-shear stress and the micro-stress in ligament L₁ can be derived as

$$\frac{\tau_{xy}^*}{\sigma_u} = \frac{1}{\left| \sin 2\theta \pm 3\frac{c}{h} \cos 2\theta \right| \left(\frac{c}{h} \right)^2} \quad (3.39)$$

In the same manner, the ratio of the applied shear stress and the maximum stress in ligament L₂ can be derived as

$$\frac{\tau_{xy}^*}{\sigma_u} = \frac{1}{\left| -\sin 2\theta \pm 3\frac{c}{h} \cos 2\theta \right| \left(\frac{c}{h} \right)^2} \quad (3.40)$$

The macroscopic shear strength (maximum shear stress) is plotted as a function of orientation θ in Figure 5.3. The maximum stress is symmetric about $\theta=45^\circ$.

Maximum strength with various crack angles when shear stress is applied

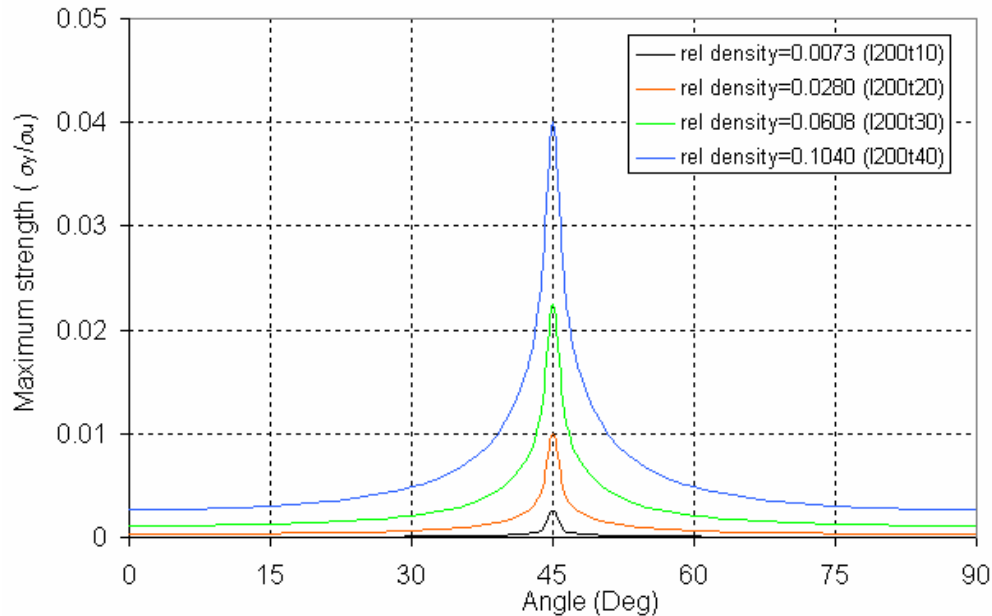


Figure 3.18 Variation of maximum shear stress (shear strength) as a function of angle between the xy coordinate system and the principal material directions

Mode I Fracture Toughness of Inclined Cracks

The procedures for predicting the fracture toughness of angled cracks (cracks inclined at an angle to the material principal directions) are very similar to that described in the preceding sections. The only change is in the material elastic constants which have to be transformed from the material principal directions to the global xy coordinate system. The stress fields under Mode I fracture for various crack angles are shown in Figure 3.19.

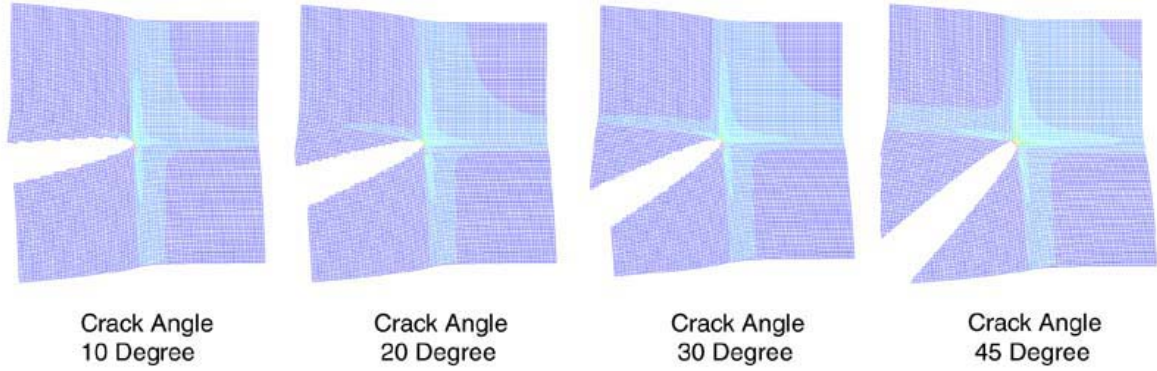


Figure 3.19 Stress distribution with various crack angles for Mode I fracture

The variation of Mode I fracture toughness with crack orientation is shown in Fig 3.20 for various relative densities. It may be noted that the variation of Mode I fracture toughness with θ is very similar to that of tensile strength shown in Fig. 3.17 with the results being symmetric about $\theta=45^\circ$.

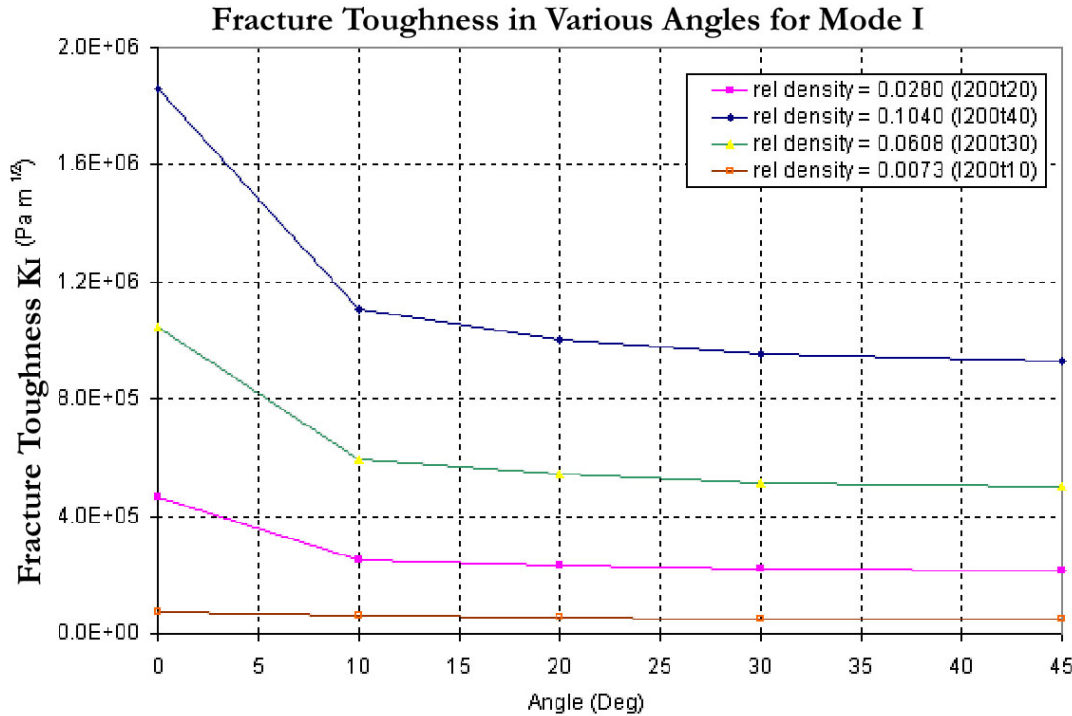


Figure 3.20 Mode I fracture toughness for various crack angles with respect to the principal material direction

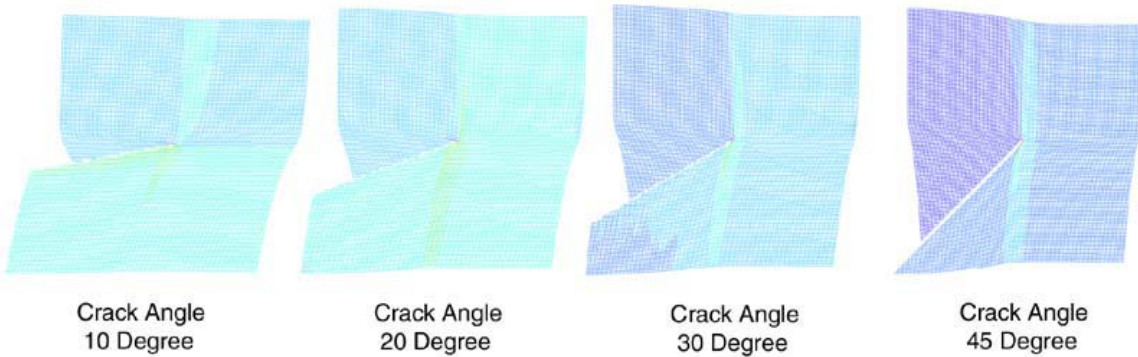


Figure 3.21 Stress distribution for various angled cracks under Mode II fracture

The stress field for various angled cracks under Mode II fracture is shown in Figure 3.21.

The variation of Mode II fracture toughness is shown in Figure 3.22. Again one can note the similarities in the variation of K_{IIc} and shear strength presented in Fig. 3.18

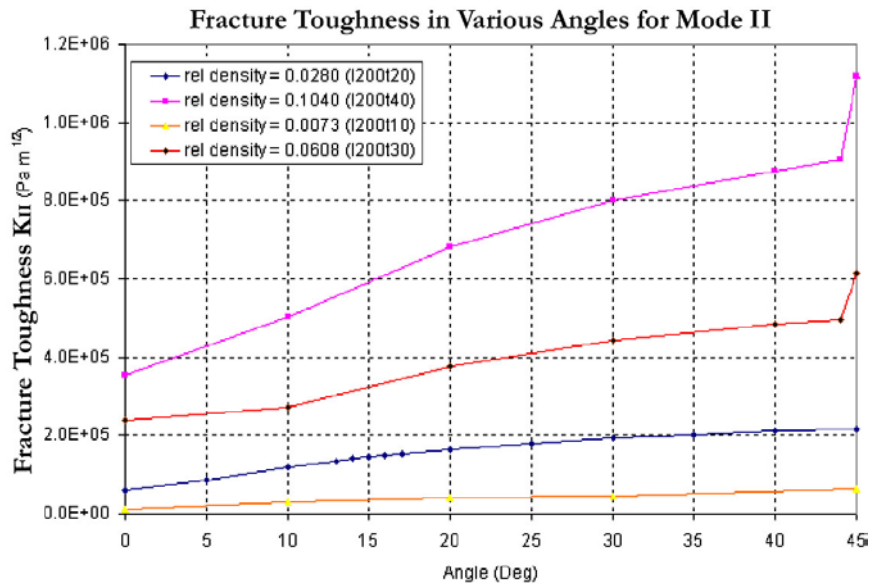


Figure 3.22 Mode II fracture toughness for various crack angles with respect to the principal material direction

CHAPTER 4

FRACTURE TOUGHNESS OF CARBON FOAM

Material Properties of Carbon Foam

From the SEM image of low-density carbon foam shown in Figure 1.1, one can note that the cells are irregularly sized and spaced. The cell size is measured to be in the range of 1 to 2 mm. Mechanical properties of the carbon foam as reported by Touchstone Research Laboratory, Inc., manufacturers of the foam, are shown in Table 4.1. The solidity (relative density) is determined by dividing, ρ^* , density of the foam, by ρ_s , the density of solid carbon that make the struts or the cell walls. The densities of various forms of carbon are given in Table 4.2. The solidity of the carbon foam used in the present study was based on the value of solid density $\rho_s = 2,250 \text{ kg/m}^3$, and the solidity is determined as 0.1312.

Table 4.1 Mechanical properties of carbon foam

Elastic Modulus (E^*)	123.79 MPa
Tensile strength (σ_u^*)	3.5805 MPa
Density (ρ^*)	295.3 kg/m ³

Table 4.2 Densities of various forms of carbon

Diamond (C Wt. %100)	3,510 kg/m ³
Graphite carbon fiber (C Wt. %100)	2,250 kg/m ³
Zoltec Pane 30MF carbon fiber (C Wt. % 99.5)	1,750 kg/m ³

Mode I Fracture Toughness Test (4-Pt. Bending Tests)

There are several methods available for measuring the fracture toughness of cellular materials. Compact tension test (CT), Single edge notched bend test (SENB) and

Double edge notched tension test (DENT) performed by Fowlkes [6] are some of the tests that are suitable for foam materials. In the present study, we chose the single edge notched four-point bend specimens for measuring the fracture toughness of carbon foams. It was thought that the four-point bending test would yield more accurate and repeatable results as the crack is in a region under constant bending moment and no transverse shear force. Hence small offset of the loading point with respect to the crack location will not significantly affect the results.

The specimen dimensions are depicted in Figure 4.1. The height of the specimen was about 50 mm and the crack length was about 25 mm. Individual specimen dimensions are given in Table 4.3. A notch was cut using a diamond saw, and then a razor blade was used to sharpen the crack tip. The crack length was the distance of the crack tip from the bottom surface edge of the beam. The tests were conducted under displacement control in a material testing machine at the rate of 0.5 mm/min (Figure 4.2). Load-deflection diagrams are given in Figure 4.3. It may be noted from the curves that the crack propagated instantaneously and the specimens failed in a brittle manner. The fracture loads for various specimens are listed in Table 4.3. The Mode I fracture toughness was calculated from the load at failure using the following formula [3]:

$$K_I = \sigma_\infty \sqrt{\pi a} \left(1.12 - 1.39 \frac{a}{w} + 7.3 \frac{a^2}{w^2} - 13 \frac{a^3}{w^3} + 14 \frac{a^4}{w^4} \right) \quad (4.1)$$

where the maximum bending stress σ_∞ in the uncracked beam is determined by

$$\sigma_\infty = \frac{M \bar{y}}{I} = \frac{M \frac{w}{2}}{\frac{B w^3}{12}} = \frac{6M}{B w^2} \quad (4.2)$$

In Eq. 4.2, M is the constant bending moment in the central region, h is the height of the specimen and B is the width. The bending moment M is given by $M=Pd/2$, where d is distance between one of the top loading points and the corresponding bottom support as shown in Figure 4.2. The results for fracture toughness are listed in Table 4.3. For the carbon foam samples tested the average Mode I fracture toughness is found to be 0.1337 MPa m^{1/2} with a standard deviation of 0.011 MPa m^{1/2} (about 8%).

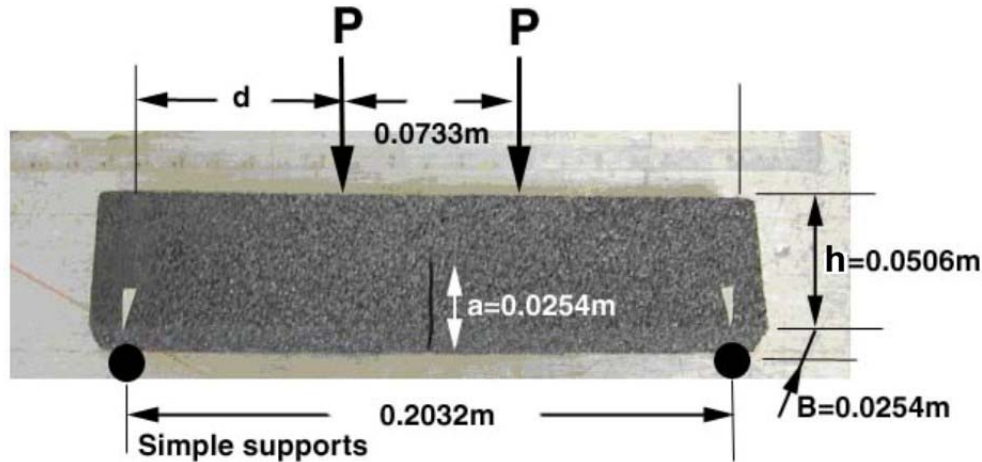


Figure 4.1 SENB specimen geometry

Table 4.3 Fracture toughness with specimen properties of carbon foam

Specimen	Span L (m)	Height h (m)	Width B (m)	Crack length a (m)	Density (Kg/m ³)	Fracture Load (N)	K_{Ic} (MPa m ^{1/2})
IF06	0.2284	0.0512	0.0255	0.0264	284	100.9	0.1315
IF07	0.2291	0.0500	0.0255	0.0252	301	112.0	0.1458
IF09	0.2290	0.0507	0.0255	0.0259	292	92.54	0.1201
IF10	0.2290	0.0506	0.0256	0.0261	297	105.8	0.1372

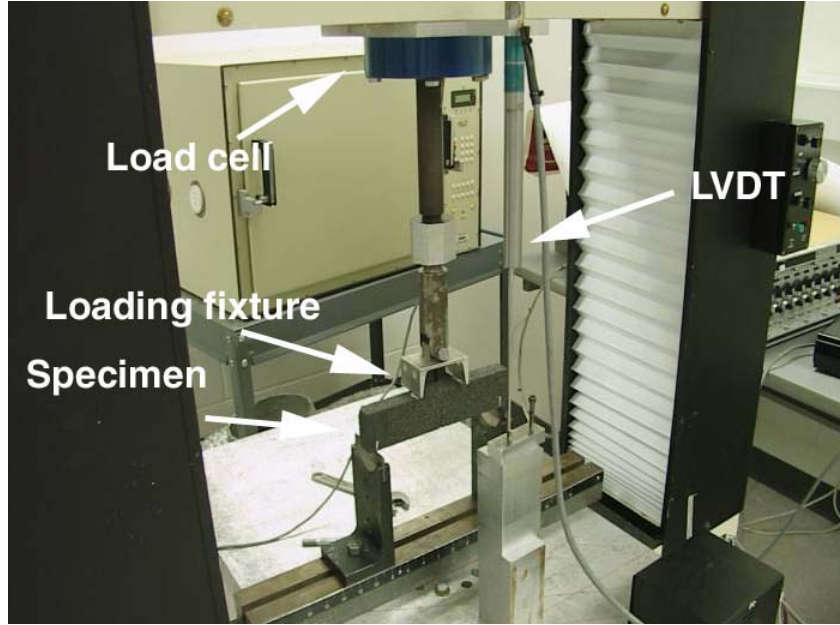


Figure 4.2 Four-point bending test setup on a material testing machine

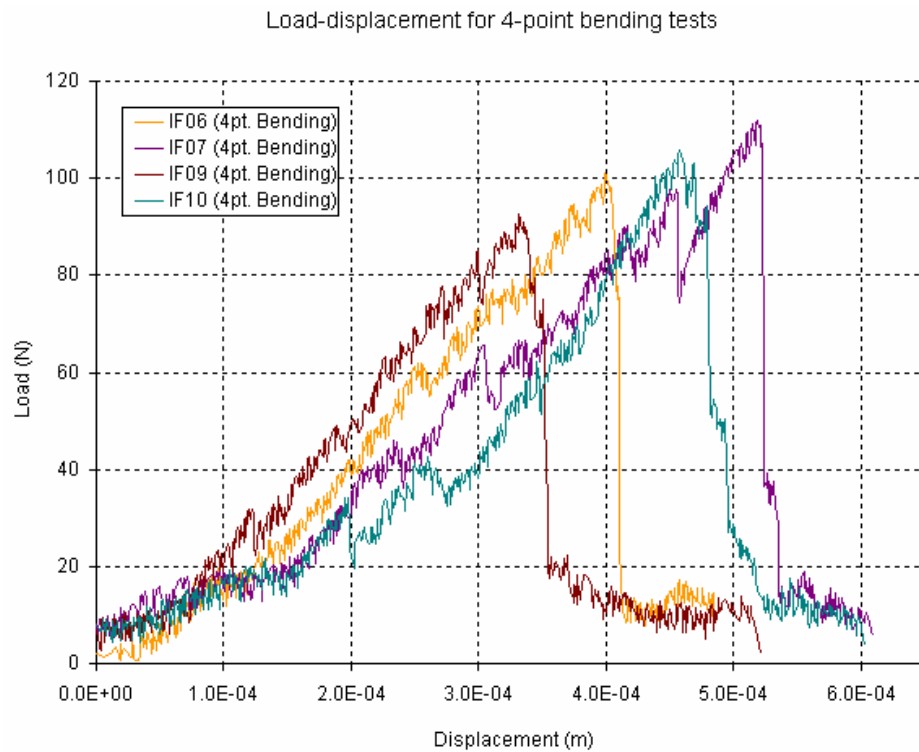


Figure 4.3 Load-displacement curves of four-point bending tests on carbon foam

Finite Element Analysis of Fracture Toughness

Unit Cell of Carbon Foam – Solid Model

The first step in simulating the crack propagation in carbon foam is to idealize the microstructure of the foam. The unit-cell is assumed as a perfect cube of side c in Figure 4.4. The foam model is created by placing a spherical void (bubble) at the center of the cube. By varying the radius of the bubble R , foams in various solidity can be modeled. A relation between the solidity and the R/c ratio can be derived in Appendix A:

$$\frac{\rho^*}{\rho_s} = \frac{4 + \pi}{4} + \frac{8}{3}\pi\left(\frac{R}{a}\right)^3 - 3\pi\left(\frac{R}{a}\right)^2 \quad (4.3)$$

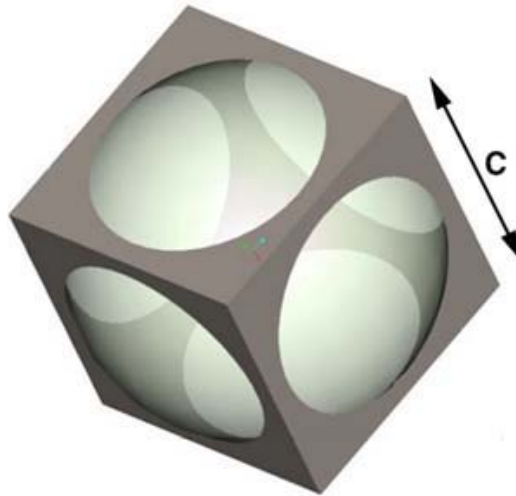


Figure 4.4 Unit cell of solid model

The average dimension of the unit-cell was obtained from the SEM images of the cross section of carbon foam. Then, the radius of the spherical void can be determined from the solidity of the foam. The Pro/Engineering®, modeling application, was used to model the unit-cell and calculate the solid volume. In the present study, the unit-cell dimension c is taken as 1.8 mm and the solidity as 0.1312.

The strength of the solid carbon in the foam can be easily estimated from the tensile strength of the carbon foam, which is measured experimentally. The relation between the foam tensile strength and the solid carbon strength is given by

$$\sigma_{us} = \sigma_u^* \frac{c^2}{A_{\min}} \quad (4.4)$$

where A_{\min} is the minimum cross sectional area of the struts in the carbon foam normal to the principal material axis. It should be noted that the tensile strength of the foam is for a direction parallel to one of the principal material axes. The area A_{\min} was obtained from the modeling software and it was equal to $= 7.146 \times 10^{-8} \text{ mm}^2$. Substituting the dimensions of the unit.cell and the measured carbon foam tensile strength, the strength of solid carbon was estimated as 162 Mpa. The procedure for determining the Young's modulus and tensile strength of the solid carbon is as follows.

Micromechanics Analysis for Young's Modulus and Shear Modulus

The Young's modulus E_s of solid carbon was estimated by a trial and error method. An initial value for E_s is assumed and the elastic constants of the carbon foam are determined by using the micromechanical methods developed by Sankar et al. [4]. Then the value of E_s can be scaled to match the micromechanical results for E^* to the experimentally measured E^* . The unit-cell was modeled by using 4-noded tetrahedral solid elements. Due to symmetry only a portion of the unit-cell was modeled and periodic boundary conditions were imposed such that only one of the macro-strains is non zero [4]. We assume a value for E_s and v_s , and the forces required to deform the unit cell are calculated from the nodal reactions. From the forces the macro-stresses can be computed. For example

$$\sigma_x^* = \frac{\sum F_x}{c^2}, \quad \sigma_y^* = \frac{\sum F_y}{c^2} \quad (4.5)$$

where $\sum F_x$ represents the sum of all nodal forces on a face normal to the x axis. Similary $\sum F_y$ is the sum of all the nodal forces F_y on the face normal to the y axis.

The carbon foam is assumed as an orthotropic material and the macro-stresses and strains are substituted in the constitutive relation to obtain the compliance coefficients S_{ij} . From the S matrix the elastic constants can be estimated using the following relations:

$$\begin{aligned} \begin{Bmatrix} \varepsilon_x^* \\ \varepsilon_y^* \\ \varepsilon_z^* \end{Bmatrix} &= \begin{Bmatrix} S_{11} & S_{12} & S_{12} \\ S_{12} & S_{11} & S_{12} \\ S_{12} & S_{12} & S_{11} \end{Bmatrix} \begin{Bmatrix} \sigma_x^* \\ \sigma_y^* \\ \sigma_z^* \end{Bmatrix} \\ \begin{Bmatrix} \frac{1}{E_x} & -\frac{\nu_{yx}}{E_y} & -\frac{\nu_{zx}}{E_z} \\ -\frac{\nu_{xy}}{E_x} & \frac{1}{E_y} & -\frac{\nu_{zy}}{E_z} \\ -\frac{\nu_{xz}}{E_x} & \frac{\nu_{yz}}{E_y} & \frac{1}{E_z} \end{Bmatrix} &= \begin{Bmatrix} S_{11} & S_{12} & S_{12} \\ S_{12} & S_{11} & S_{12} \\ S_{12} & S_{12} & S_{11} \end{Bmatrix} \end{aligned} \quad (4.6)$$

The FE model contained approximately 100,000 solid tetrahedral elements. A displacement $u_y=1$ was applied to the top surface of a unit cell (Figure 4.5). The contour plot of maximum principal stresses is depicted in Figure 4.5.

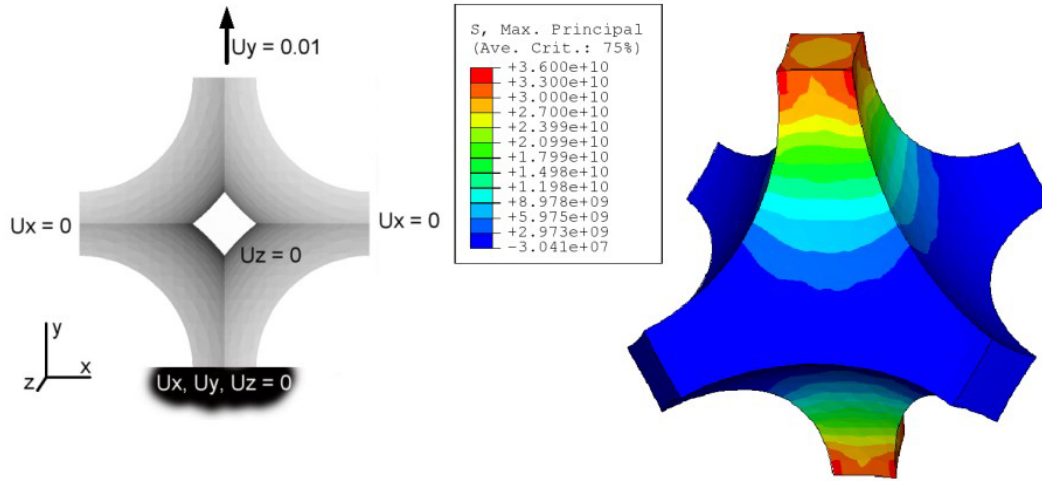


Figure 4.5 Boundary conditions on the unit-cell surfaces and maximum principal stress distribution when the unit-cell is stretched in the y -direction

For the sake of simplicity no attempt was made to estimate the Poisson's ratio ν_s using the micro-mechanical methods and it was assumed to be equal to 0.17 based on a previous analysis. Based on the foam properties given in Table 4.1 and the unit-cell size c of 1.8mm, the Young's modulus of solid carbon E_s was estimated to be 2.6 GPa. Using this value for E_s the Young's modulus of carbon foams of various solidities was calculated using the FE model and they are shown in Figure 4.7.

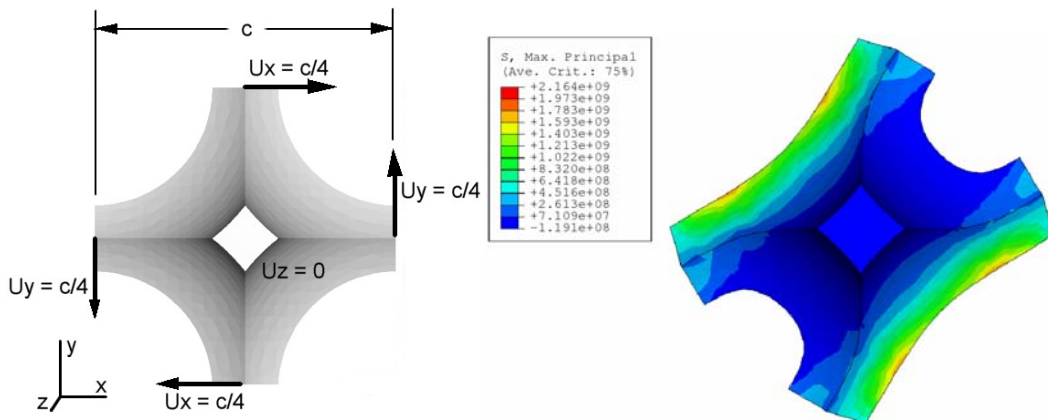


Figure 4.6 Boundary conditions on the unit-cell surfaces and maximum principal stress distribution when the unit-cell is stretched in the y -direction

The shear modulus was also calculated using the micromechanics analysis developed by Marrey and Sankar [4]. The variation of shear modulus as function of solidity is shown in Figure 4.8.

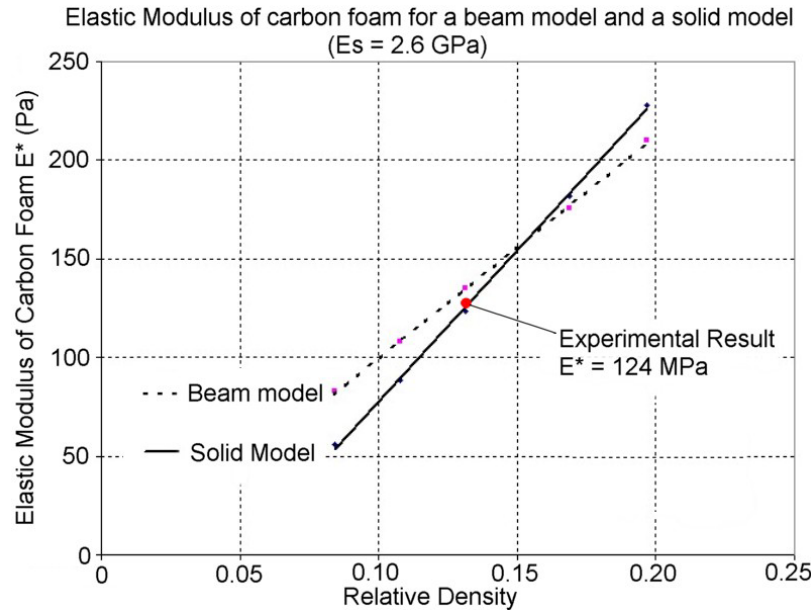


Figure 4.7 Elastic modulus E^* as a function of relative density (solidity) for $E_s = 2.6$ GPa.

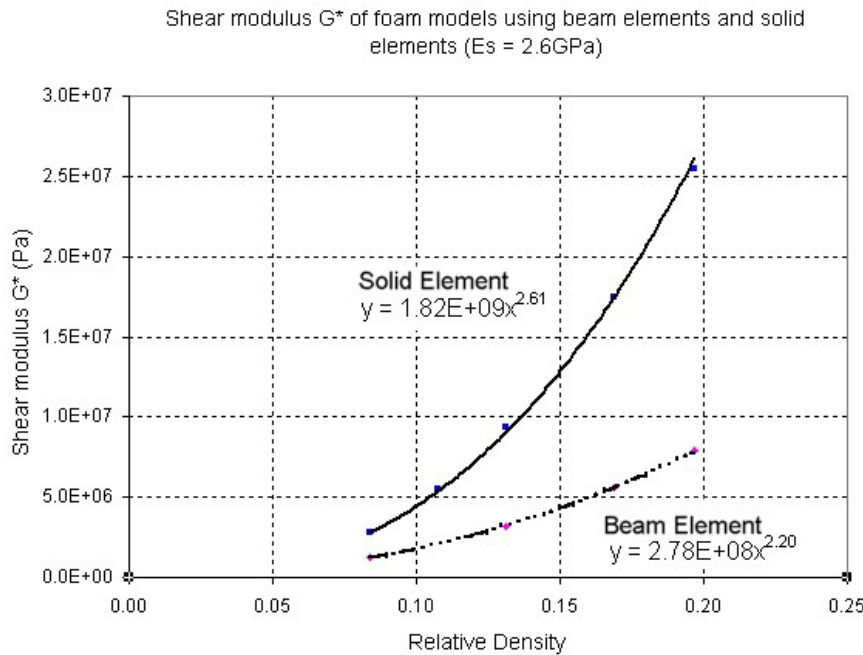


Figure 4.8 Shear modulus G^* as a function of relative density (solidity) for $E_s = 2.6$ GPa.

Unit Cell of Carbon Foam – Beam Model

In addition to the solid model described in the preceding section a simple lattice model was also attempted. In this model the foam is assumed to be made up of struts arranged in a cubic lattice pattern. The length of the strut was equal to the unit-cell dimension c in Figure 4.9. The struts were assumed to be uniform square cross section beam and their dimensions were determined from the relative density of the foam.

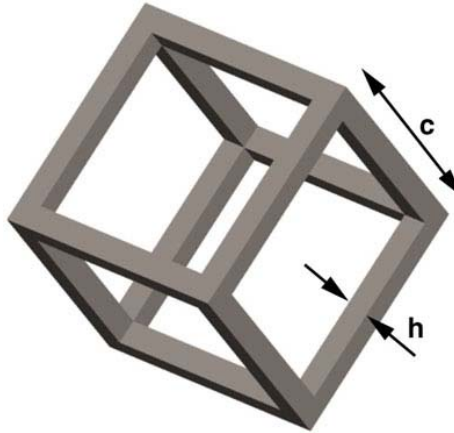


Figure 4.9 Unit cell of beam model

From the Eq. (2.11), the wall thickness h is determined to be 0.4086 mm for a solidity of 0.1312 and $c = 1.8$ mm. Since this beam model is composed as a simplest shape, FE methods are not necessary to determine the relation between the solid properties and foam properties. Analytical expressions for various elastic properties have been derived earlier section. Based on the Eq. (2.1) and Eq. (2.4), the Young's modulus E_s and the strength σ_{us} are found to be 2.4 MPa and 69.5 MPa, respectively. The variation of E^* and G^* with the solidity for the beam model are shown, respectively, in Figures 4.7 and 4.8.

Fracture Toughness Estimation of the Solid Model

In this section, we describe a finite element based micromechanics model to estimate the fracture toughness of the cellular solid. The crack is assumed to be parallel to one of the principal material axes. The crack is created by breaking the ligaments of the unit cell (Figure 4.10). To determine the fracture toughness, a small region of the foam around the crack tip is modeled using finite elements. Only Mode I fracture is considered in the present study. The boundary of the cellular solid is subjected to displacement boundary conditions (u_x and u_y) corresponding to a unit K_{Ic} , i.e., $K_I = 1$. The displacement components in the vicinity of a crack tip in an orthotropic solid can be found in Appendix B.

The maximum tensile stress in the unit-cells corresponding to unit stress intensity factor is calculated from the FE model. In the case of three-dimensional solid model the maximum stress is obtained as an output of the FE program. From the result the value of K_I that will cause rupture of the strut is estimated, which then is taken as the fracture toughness of the cellular solid.

The solid model used 42 cells with 135,000 solid tetrahedral elements as shown in Figure 4-10. The maximum principal stress distribution is shown in Figure 4.10. When unit K_I was applied to the crack tip, maximum principal stress was found equal to 1,463 Pa. Then the fracture toughness is obtained from the strength of the solid carbon ($\sigma_{us} = 0.162 \text{ MPa}$) as

$$K_{IC} = \frac{\sigma_{us}}{\sigma_{\max}} = \frac{162 \times 10^6}{1463} = 0.11 \text{ MPa}\sqrt{m} \quad (4.12)$$

Comparing Eq. (4-12) with the results of fracture toughness experiments (Table 4.3), the difference is about 16%. One reason for the difference could be the small number of cells used in the FE simulation. The FE model was used to study the variation of fracture toughness with relative density and the resulting relationship is shown in Figure 4.11. Gibson and Ashby [2] provide analytical results for fracture toughness for open-cell foam as given below:

$$\frac{K_{IC}^*}{\sigma_{us} \sqrt{\pi c}} = 0.65 \left(\frac{\rho^*}{\rho_s} \right)^{3/2} \quad (4.13)$$

where σ_{us} is the tensile strength of the solid. Using the above formula the fracture toughness for the carbon foam considered in this study can be obtained as $0.162 \text{ MPa}\sqrt{\text{m}}$. The variation of K_{Ic} according to Eq. (4-13) is presented in Figure 4.11.

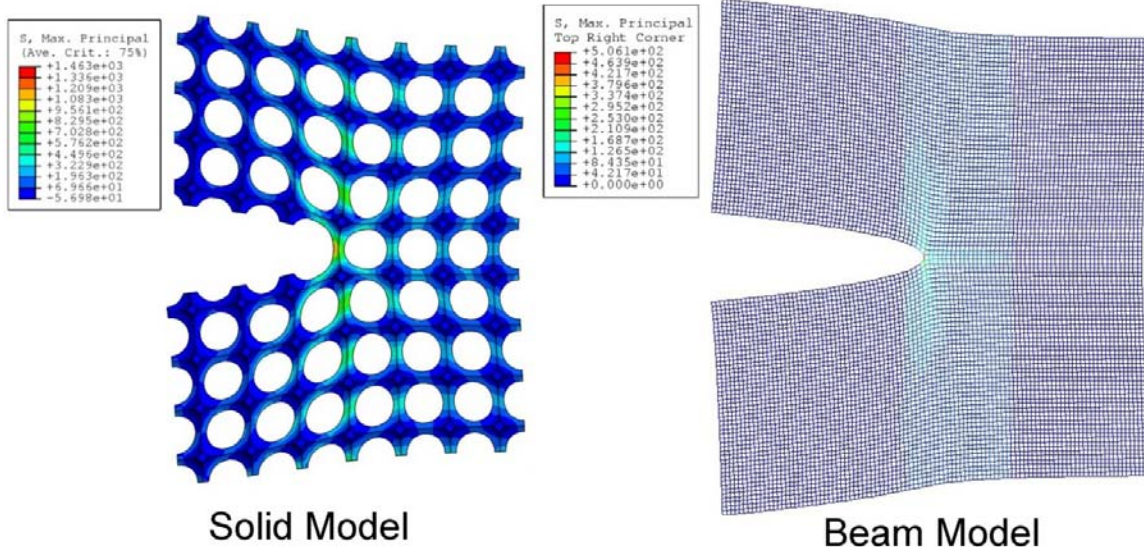


Figure 4.10 Maximum principal stress distribution of solid and beam models for a unit K_I at the crack tip

Fracture Toughness of the Beam Model

The procedure for simulating fracture using the beam model is the same as that for the FE solid model. The beam model of carbon foam (Figure 4.10) consisted of

10,000 cells using approximately 20,000 beam elements. When using the beam model, the rotational degree of freedom at each node of the beam element on the boundary of the solid is left as unknown and no couples are applied at these nodes. The maximum principal stress distribution in the beam model for $K_I=1$ is shown in Figure 4.10. The maximum principal stress for a unit K_I was found to be equal to 506 Pa. Therefore, the fracture toughness can be estimated as

$$K_{IC} = \frac{\sigma_{us}}{\sigma_{max}} = \frac{69 \times 10^6}{506} = 0.137 \text{ MPa}\sqrt{m} \quad (4.14)$$

The difference between the experimental result and that from the beam model is only 3%. The beam model was also used to study the variation of fracture toughness with the solidity and it is presented in Figure 4.11.

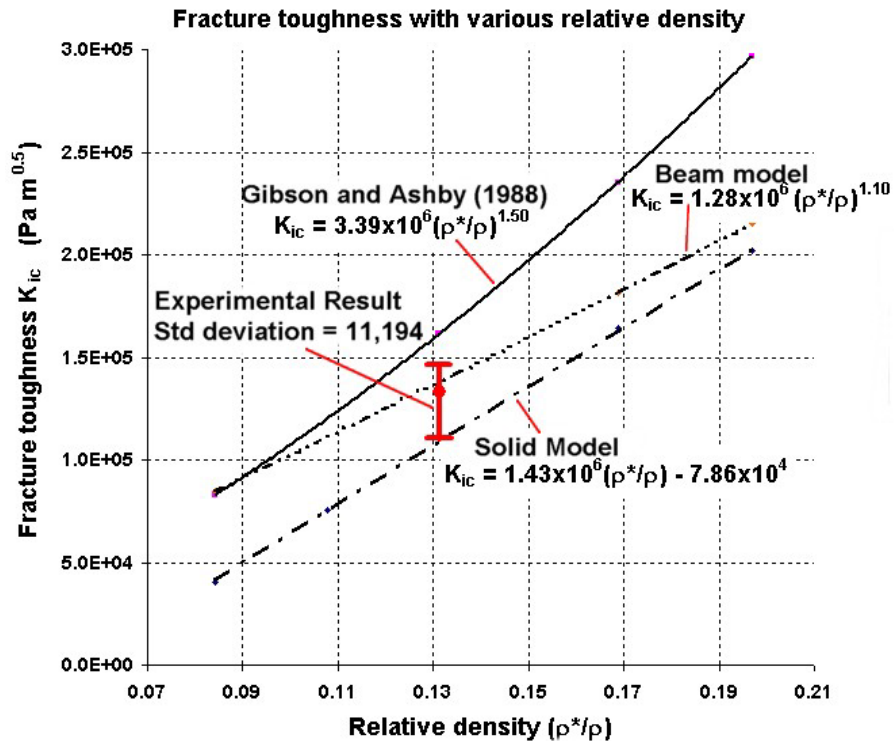


Figure 4.11 Variation of fracture toughness of carbon foam with relative density

CHAPTER 5 RESULTS AND DISCUSSION

Elastic Constants of Open-cell Foam

Young's modulus for carbon foam in the principal material direction is estimated to be 2.09 GPa from the FE micro-mechanics and 2.07 GPa based on analytical solutions. Shear modulus is predicted as 10.245 MPa from FE analysis and 10.350 MPa from analytical solution. Difference between analytical and numerical results is 0.96% for elastic modulus and 1.01% for shear modulus. For open-cell foam model, analytical solutions and FE solutions for elastic constants show good agreement.

Numerical Analysis of Fracture Toughness

A Finite Element method based micro-mechanics method was developed to predict the fracture toughness of cellular materials. A portion of material around the crack tip was modeled using finite elements. Boundary displacements calculated using orthotropic fracture mechanics were applied to the FE model. The stress intensity factor corresponding to the failure of the crack tip strut was taken as the fracture toughness of the cellular medium. It has been found that the fracture toughness is a strong function of relative density of the foam, however it also depends on the strut dimensions and spacing. Based on the FE results an analytical model was developed to predict the fracture toughness. A simple empirical formula has been derived for the effective length ahead of the crack tip that contributes to the crack tip ligament forces and bending moment. For the type of cellular medium considered in this study the fracture toughness can be

expressed in the form of power law of the type where K is fracture toughness and R is relative density. The constants a and b for Mode I and Mode II are presented in Table 5.1

Table 5.1 Constants of fracture toughness curves

	Constant length of cell edge with various wall thickness		Constant wall thickness with various length of cell edge	
	A	b	a	b
Mode I	1.961×10^7	1.045	7.82×10^6	0.788
Mode II	6.95×10^6	1.32	2.76×10^6	1.070

The effective length l ahead of the crack-tip is expresses as $l=\alpha c$. The constant α was evaluated analytically using the results for fracture toughness obtained using the FE micro-mechanics models. It has been found that α depends only on relative density and is independent of cell length or strut cross sectional dimensions.

Fracture Toughness with an Angle Crack

Variation of strength under combined loading for open-cell foams was evaluated analytically. The results were used to determine the tensile and shear strength when the loads are applied at an angle to the principal material directions. FE micro-mechanics simulations were performed for inclined cracks. Mode I fracture toughness is maximum at 0° and Mode II fracture toughness is maximum at 45° to the principal material direction.

Fracture Toughness of Carbon Foam

Four point bend tests were performed on SENB specimens made of carbon foam, and their Mode I fracture toughness was measured. In addition to the experimental approach, a finite element based micromechanics has been developed to predict the fracture toughness. Two micro-mechanical models were developed to simulate Mode I fracture. Both models assumed a cube as the unit-cell of the foam. In the first model solid finite elements were used to model the foam. The measured density of the carbon foam

was used in determining the void size in the micromechanical model. Young's modulus and tensile strength of the solid carbon were also determined from the corresponding values of the carbon foam measured experimentally. A small region surrounding the crack tip was modeled using finite elements. The crack was assumed parallel to one of the principal material directions. Boundary displacements were calculated using linear elastic fracture mechanics for orthotropic materials. From the FE simulation the stress intensity factor K_I that will cause the failure of the crack-tip elements was determined, and this was taken as the fracture toughness of the cellular material shown in Table 5.2. The agreement between the test results and numerical results are good indicating micro-mechanics can be a powerful tool in predicting the fracture behavior of foams and other cellular solids.

Table 5.2 Results of fracture toughness

	K_{ic} (MPa m ^{1/2})	% Difference from Experiment
Beam Model	0.137	3
Solid Model	0.110	17
Gibson & Ashby	0.162	21
Experimental	0.132	

APPENDIX A
ANALYTICAL METHOD TO ESTIMATE THE SOLIDITY OF SOLID MODEL

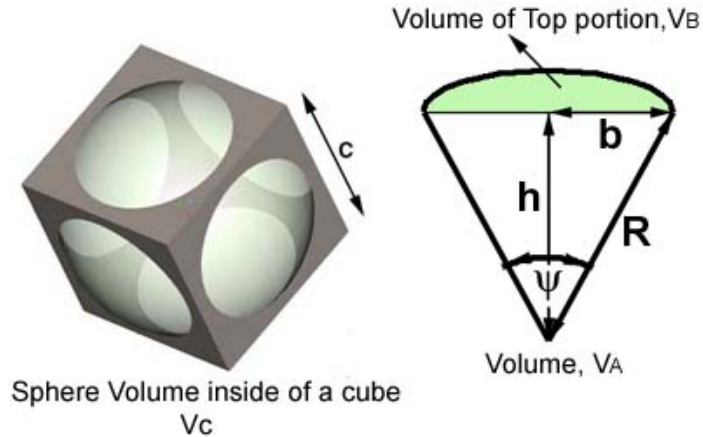


Figure A.1 Unit cell of solid model

To estimate the solidity of porous medium in the solid model, the volume of the pore (void) left inside the unit-cell needs to be determined. In order to do that, the volume of top portion V_B in Fig. A1 is subtracted from entire sphere volume of a void. The volume V_A is obtained as

$$V_A = \frac{\psi}{3} R^3 \quad (\text{A.1})$$

where Ψ is solid angle. The solid angle can be obtained as follows:

$$\psi = \frac{dA}{R^2} \quad (\text{A.2})$$

$$dA = 2\pi r dr \cos\theta \quad (\text{A.3})$$

$$d\psi = \frac{dA}{h^2 + r^2} = \frac{2\pi r dr \cos\theta}{h^2 + r^2} = \frac{2\pi r h dr}{(h^2 + r^2)^{3/2}} \quad (\text{A.4})$$

Integrating both sides,

$$\int_0^b d\psi = \int_0^b \frac{2\pi r h dr}{(h^2 + r^2)^{\frac{3}{2}}} \quad (\text{A.5})$$

$$\psi = 2\pi h \left[\frac{1}{h} - \frac{1}{R} \right] \quad (\text{A.6})$$

By substitute Eq. (A6) into Eq. (A1), V_A is obtained as follows;

$$V_A = \frac{\psi}{3} R^3 = \frac{2\pi}{3} h R^3 \left[\frac{1}{h} - \frac{1}{R} \right] = \frac{2\pi R^2}{3} [R - h] \quad (\text{A.7})$$

The volume of the top portion V_B can be obtained by subtracting the volume of the cone from V_A

$$V_B = \frac{2\pi R^2}{3} [R - h] - \frac{1}{3} \pi b^2 = \frac{2\pi R^3}{3} - \pi R^2 h + \frac{1}{3} \pi h^3 \quad (\text{A.8})$$

The volume of the pore left inside the unit-cell is derived as V_C ,

$$V_c = \frac{4\pi R^3}{3} - 6V_B = \frac{4\pi R^3}{3} - 4\pi R^3 + 3\pi R^2 a - \frac{\pi a^3}{4} \quad (\text{A.9})$$

Therefore, the solidity can be obtained from its definition as:

$$\frac{\rho^*}{\rho_s} = \frac{a^3 - V_c}{a^3} = 1 - \frac{V_c}{a^3} = 1 - \frac{1}{a^3} \left[\frac{4\pi R^3}{3} - 4\pi R^3 + 3\pi R^2 a - \frac{1}{4} \pi a^3 \right] \quad (\text{A.10})$$

For open cell model, the equation is only valid in the range where R is the radius of the sphere in Fig. A1. After simplifying the equation, the solidity can be expressed in terms of the ratio R/a in the form of a polynomial:

$$\frac{\rho^*}{\rho_s} = \frac{4 + \pi}{4} + \frac{8}{3} \pi \left(\frac{R}{a} \right)^3 - 3\pi \left(\frac{R}{a} \right)^2 \quad (\text{A.11})$$

APPENDIX B

CRACK TIP DISPLACEMENT FIELDS FOR ORTHOTROPIC MATERIAL

The open-cell foam is considered as a homogeneous orthotropic material. The principal material directions are parallel to the 1 and 2 axes. Assuming the Poisson's ratio is negligible, the stress-stain relations in the 1-2 plane are given in the matrix form below.

$$\begin{Bmatrix} \varepsilon_1 \\ \varepsilon_2 \\ \gamma_{12} \end{Bmatrix} = [S][\sigma] = \begin{Bmatrix} \frac{1}{E^*} & 0 & 0 \\ 0 & \frac{1}{E^*} & 0 \\ 0 & 0 & \frac{1}{G^*} \end{Bmatrix} \begin{Bmatrix} \sigma_1 \\ \sigma_2 \\ \tau_{12} \end{Bmatrix} \quad (\text{B.1})$$

When the cellular medium is oriented at an angle to the principal material axes, the stress-stain relation can be transformed from the 1-2 plane to the x - y plane by using transformation matrix $[T]$. The angle θ is the angle the 1 direction makes with the x axis.

$$[T] = \begin{bmatrix} \cos^2 \theta & \sin^2 \theta & 2\sin \theta \cos \theta \\ \sin^2 \theta & \cos^2 \theta & -2\sin \theta \cos \theta \\ -\sin \theta \cos \theta & \sin \theta \cos \theta & \cos^2 \theta - \sin^2 \theta \end{bmatrix} \quad (\text{B.2})$$

$$\begin{Bmatrix} \sigma_x \\ \sigma_y \\ \sigma_z \end{Bmatrix} = [T] \begin{Bmatrix} \sigma_1 \\ \sigma_2 \\ \sigma_3 \end{Bmatrix} \quad (\text{B.3})$$

By applying the transformation, the compliance matrix in the x - y coordinates is written as

$$\begin{Bmatrix} \varepsilon_x \\ \varepsilon_y \\ \gamma_{xy} \end{Bmatrix} = [T]^T [S] [T] \begin{Bmatrix} \sigma_x \\ \sigma_y \\ \tau_{xy} \end{Bmatrix} = \begin{Bmatrix} \bar{S}_{11} & \bar{S}_{12} & \bar{S}_{16} \\ \bar{S}_{12} & \bar{S}_{22} & \bar{S}_{26} \\ \bar{S}_{16} & \bar{S}_{26} & \bar{S}_{66} \end{Bmatrix} \begin{Bmatrix} \sigma_x \\ \sigma_y \\ \tau_{xy} \end{Bmatrix} \quad (\text{B.4})$$

The components of the matrix can be obtained in terms of compliance terms referred to the 1-2 axes as follows:

$$\bar{S}_{11} = S_{11} \cos^4 \theta + (2S_{12} + a_{66}) \sin^2 \theta \cos^2 \theta + S_{22} \sin^4 \theta \quad (\text{B.5a})$$

$$\bar{S}_{12} = S_{12} (\sin^4 \theta + \cos^4 \theta) + (S_{11} + S_{22} - S_{66}) \sin^2 \theta \cos^2 \theta \quad (\text{B.5b})$$

$$\bar{S}_{22} = S_{11} \sin^4 \theta + (2S_{12} + S_{66}) \sin^2 \theta \cos^2 \theta + S_{22} \cos^4 \theta \quad (\text{B.5c})$$

$$\bar{S}_{16} = (2S_{11} - 2S_{12} - S_{66}) \sin \theta \cos^3 \theta - (2S_{22} - 2S_{12} - S_{66}) \sin^3 \theta \cos \theta \quad (\text{B.5d})$$

$$\bar{S}_{16} = (2S_{11} - 2S_{12} - S_{66}) \sin^3 \theta \cos \theta - (2S_{22} - 2S_{12} - S_{66}) \sin \theta \cos^3 \theta \quad (\text{B.5e})$$

$$\bar{S}_{11} = 2(2S_{11} + 2S_{22} - 4S_{12} - S_{66}) \sin^2 \theta \cos^2 \theta + S_{66} (\sin^4 \theta + \cos^4 \theta) \quad (\text{B.5f})$$

The characteristic equation of the orthotropic material is given by

$$\bar{S}_{11} \mu^4 - 2\bar{S}_{16} \mu^3 + (2\bar{S}_{12} + \bar{S}_{66}) \mu^2 - 2\bar{S}_{22} \mu + \bar{S}_{22} = 0 \quad (\text{B.6})$$

where imaginary roots of the characteristic equation are described as ($j = 1, 2, 3, 4$).

The constant ($j = 1, 2$) can be obtained by using the equation below. The roots and are unequal roots with a positive conjugate value.

$$s_1 = \mu_1 = \alpha_1 + i\beta_1 \quad s_2 = \mu_2 = \alpha_2 + i\beta_2$$

The constants, ($j = 1, 2$) are relates to constants s as shown below.

$$p_1 = a_{11}s_1^2 + a_{12} - a_{16}s_1 \quad p_2 = a_{11}s_2^2 + a_{12} - a_{16}s_2$$

$$q_1 = \frac{a_{12}s_1^2 + a_{22} - a_{26}s_1}{s_1} \quad q_2 = \frac{a_{12}s_2^2 + a_{22} - a_{26}s_2}{s_2}$$

Stress components of polar and rectangular coordinates at a crack are shown in Figure B.1. The angle θ is taken positive in the counterclockwise direction. The distance r is taken from the crack tip at the point O.

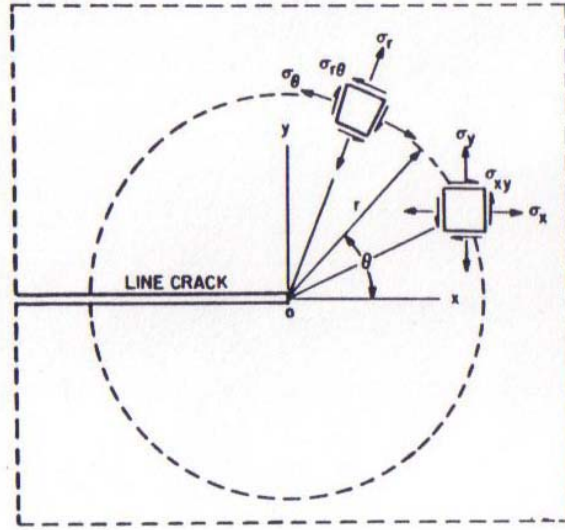


Figure B.1 Polar coordinate oriented from crack tip

The displacement components for Mode I and Mode II can be defined as

The displacement field near the crack tip for Mode I:

$$\begin{aligned} u_x &= K_I \sqrt{\frac{2r}{\pi}} \operatorname{Re} \left\{ \frac{1}{s_1 - s_2} [s_1 p_2 (\cos \theta + s_2 \sin \theta)^{1/2} - s_2 p_1 (\cos \theta + s_1 \sin \theta)^{1/2}] \right\} \\ u_y &= K_I \sqrt{\frac{2r}{\pi}} \operatorname{Re} \left\{ \frac{1}{s_1 - s_2} [s_1 q_2 (\cos \theta + s_2 \sin \theta)^{1/2} - s_2 q_1 (\cos \theta + s_1 \sin \theta)^{1/2}] \right\} \end{aligned} \quad (\text{B.7})$$

The displacement field near the crack tip for Mode II:

$$\begin{aligned} u_x &= K_{II} \sqrt{\frac{2r}{\pi}} \operatorname{Re} \left\{ \frac{1}{s_1 - s_2} [p_2 (\cos \theta + s_2 \sin \theta)^{1/2} - p_1 (\cos \theta + s_1 \sin \theta)^{1/2}] \right\} \\ u_y &= K_{II} \sqrt{\frac{2r}{\pi}} \operatorname{Re} \left\{ \frac{1}{s_1 - s_2} [q_2 (\cos \theta + s_2 \sin \theta)^{1/2} - q_1 (\cos \theta + s_1 \sin \theta)^{1/2}] \right\} \end{aligned} \quad (\text{B.8})$$

REFERENCES

1. Fowlkes, Charles W., "Fracture Toughness Tests of a Rigid Polyurethane Foam," *International Journal of Fracture*, Volume 10, No. 1, March 1974, pp. 99-108.
2. Gibson, L.J. and Ashby, M.F., *Cellular Solids: Structure and Properties*, Second Edition, Cambridge University Press, Cambridge, United Kingdom, 1988.
3. Hellan, K., *Introduction to Fracture Mechanics*, McGraw-Hill, NY, 1984, p. 244.
4. Marrey, Ramesh V. and Sankar, Bhavani V., "Micromechanical Models for Textile Structural Composites," NASA contractor report, 198229, October 1995.
5. Sih, G.C. and Liebowitz, H., "Mathematical Theories of Brittle Fracture," *Fracture-An Advanced Treatise*, Volume 2, Liebowitz, H., Ed., Academic Press, New York, 1968, pp. 67-190.

BIOGRAPHICAL SKETCH

Sukjoo Choi was born in Seoul, Korea, on 1972. He received his Bachelor of Science degree in aerospace engineering in 1997 from the University of Minnesota at Minneapolis. He worked as a mechanical engineer in control surfaces and mechanics at the Cirrus Design, Corp., Duluth, Minnesota from 1997 to 1998. In 1998, he joined the military in Korea and served until 1998. In 2000, he was admitted to the graduate program in the Department of Aerospace Engineering, Mechanics & Engineering Science at the University of Florida, Gainesville, Florida. Sukjoo Choi will be pursuing his doctoral studies in the field of composite materials and structures in the Department of Mechanical & Aerospace Engineering at the University of Florida.